Neurobiology of Disease

An Ascending Excitatory Circuit from the Dorsal Raphe for Sensory Modulation of Pain

Di Liu,[1,2,3]* Su-Wan Hu,[1,2]* Di Wang,[1,2] Qi Zhang,[1,2] Xiao Zhang,[1,2] Hai-Lei Ding,[1,2] and Jun-Li Cao[1,2,4,5]

[1]Jiangsu Province Key Laboratory of Anesthesiology, Xuzhou Medical University, Xuzhou 221004, China, [2]Jiangsu Province Key Laboratory of Anesthesia and Analgesia Application Technology, Xuzhou Medical University, Xuzhou 221004, China, [3]Department of Anesthesiology, Shanghai General Hospital, Shanghai Jiao Tong University School of Medicine, Shanghai 200080, China, [4]Department of Anesthesiology, The Affiliated Hospital of Xuzhou Medical University, Xuzhou 221002, China, and [5]NMPA Key Laboratory for Research and Evaluation of Narcotic and Psychotropic Drugs, Xuzhou Medical University, Xuzhou 221004, China

The dorsal raphe nucleus (DRN) is an important nucleus in pain regulation. However, the underlying neural pathway and the function of specific cell types remain unclear. Here, we report a previously unrecognized ascending facilitation pathway, the DRN to the mesoaccumbal dopamine (DA) circuit, for regulating pain. Chronic pain increased the activity of DRN glutamatergic, but not serotonergic, neurons projecting to the ventral tegmental area (VTA) (DRN^{Glu}-VTA) in male mice. The optogenetic activation of DRN^{Glu}-VTA circuit induced a pain-like response in naive male mice, and its inhibition produced an analgesic effect in male mice with neuropathic pain. Furthermore, we discovered that DRN ascending pathway regulated pain through strengthened excitatory transmission onto the VTA DA neurons projecting to the ventral part of nucleus accumbens medial shell (vNAcMed), thereby activated the mesoaccumbal DA neurons. Correspondingly, optogenetic manipulation of this three-node pathway bilaterally regulated pain behaviors. These findings identified a DRN ascending excitatory pathway that is crucial for pain sensory processing, which can potentially be exploited toward targeting pain disorders.

Key words: **dorsal raphe; glutamate; nucleus accumbens; pain; ventral tegmental area**

Significance Statement

The dorsal raphe nucleus (DRN) in the midbrain contributes to pain processing, yet the detailed cellular and circuitry mechanisms remain largely unknown. Here, we report that chronic pain increases the activity of a specific subpopulation of DRN glutamatergic neurons, which project to the ventral tegmental area (VTA). The elevated excitability of DRN glutamatergic neurons causes the increased excitatory inputs to VTA dopamine neurons that selectively innervate the ventral part of the nucleus accumbens medial shell (vNAcMed). Optogenetic activation of the DRN-VTA-vNAcMed pathway induced neuronal plasticity in the VTA and resulted in pain hypersensitivity. These findings shed light on how ascending DRN excitatory circuit is involved in the sensory modulation of pain.

Introduction

Due to insufficient clinic treatment, chronic pain is still a leading cause of disability and burden of the disease worldwide (Cohen et al., 2021). Although studies indicate the importance of the peripheral nerve and the spinal cord in pain processing (Peirs and Seal, 2016), we have little knowledge about how brain mechanisms contribute to the development and the maintenance of chronic pain. Studies in the last few decades have identified endogenous pathways that suppressed the transmission of pain sensory signals (Ossipov et al., 2010; Cohen and Mao, 2014). Within these pathways, the dorsal raphe nucleus (DRN) is believed to play essential roles (Duggan and Griersmith, 1979; Segal, 1979; Andersen and Dafny, 1983; Wager et al., 2007; Li et al., 2016; Nissen et al., 2018).

The DRN is the largest serotonergic nucleus and supplies the majority of serotonergic projections in the brain (Baker et al., 1990; Jacobs and Azmitia, 1992). These serotonin neurons act as predominant origination for the inhibitory roles of the DRN in pain sensation (Duggan and Griersmith, 1979; Reyes-Vazquez et al., 1989; Cohen and Mao, 2014; Nissen et al., 2018;

Received May 11, 2023; revised Nov. 22, 2023; accepted Nov. 28, 2023.

Author contributions: D.L., H.-L.D., and J.-L.C. designed research; D.L., S.-W.H., D.W., Q.Z., and X.Z. performed research; D.L., S.-W.H., D.W., and Q.Z. analyzed data.

This work was supported by the following grants: The Sci-Tech Innovation 2030—Major Project—2021ZD0203100 (J.L.C.); the National Natural Science Foundation of China 81720108013, 82293641, and 82130033 (J.L.C.); National Natural Science Foundation of China 82271263 (H.L.D.); and National Natural Science Foundation of China 82001174 (D.L.).

*D.L. and S.-W.H. contributed equally to this work.

The authors declare no competing financial interests.

Correspondence should be addressed to should be addressed to Jun-Li Cao at caojl0310@aliyun.com or Hai-Lei Ding at haileimdar@yahoo.com.

https://doi.org/10.1523/JNEUROSCI.0869-23.2023

De Gregorio et al., 2019). However, the subsets of DRN neurons are heterogeneous in terms of functions (Vong et al., 2011; Liu et al., 2014; McDevitt et al., 2014; Matthews et al., 2016). The direct role and its underlying circuitry mechanism for specific DRN cell types, in particular, the barely understood nonserotonergic neurons, in regulating pain sensation have not been established.

Brain mapping studies demonstrate that the DRN forms dense neural connections with the midbrain ventral tegmental area (VTA) (McDevitt et al., 2014; Beier et al., 2015), a brain region that is critical for pain sensation regulation (Becerra et al., 2001; Wood, 2006; Woo et al., 2015). The VTA modulates pain sensation through its main projection target the NAc (Baliki et al., 2010; Gear and Levine, 2011; Imai et al., 2011; Baliki and Apkarian, 2015). Previous optogenetic (Zhang et al., 2017), pharmacological (Navratilova et al., 2012; Liu et al., 2018), and electrophysiological studies (Marinelli et al., 2005) suggested a role for the NAc-projecting VTA dopamine (VTA^{DA}-NAc) neurons in pain processing. This then raises the possibility that the DRN inputs may result in alterations in functions of the VTA-NAc pathway to participate in pain regulation. However, VTA DA neurons can be separated anatomically and functionally into heterogeneous subpopulations (Morales and Margolis, 2017), and the precise circuitry that coding pain signals remains controversial. For example, studies have demonstrated an ongoing activity of the VTA-NAc pathway in the maintenance of pain (Lee et al., 2008; Brischoux et al., 2009; Sagheddu et al., 2015; Zhang et al., 2017). While other studies showed that dopamine neuron excitability was decreased following chronic pain (Ren et al., 2016; Watanabe et al., 2018). It is unclear whether there is a separate subpopulation of mesolimbic DA neurons that shows differential properties in pain modulation.

Although the midbrain reward circuit is involved in multiple aspects of pain, in the present study, we mainly investigated how this pathway modulates pain sensation. Using the combined approaches of rabies virus with adeno-associated virus (AAV) (Beier et al., 2015; Callaway and Luo, 2015), we established a cell type-specific monosynaptic tracing of subgroups of DRN neurons innervating the VTA DA neurons projecting to separate NAc medial shell subdivisions—the ventral part of NAcMed (vNAcMed) and the dorsal part of NAcMed (dNAcMed). We precisely manipulated theses projecting specific DRN neurons and found the DRN-VTA^{DA}-vNAcMed pathway preferably promoted pain responses. Especially, this pain-facilitative effect was mediated by the glutamatergic neurons rather than the most studied serotonergic neurons within the DRN. Finally, we showed the potentiated mesolimbic excitatory synaptic transmission underlying the facilitatory roles of the DRN-VTA^{DA}-vNAcMed pathway in a chronic pain state. This work provided a mechanistic understanding of the roles of the DRN in the regulation of pain and supplied a potential target for the treatment of pain disorders.

Materials and Methods

Experimental animals

Male Vgat-IRES-Cre and wild-type C57BL/6J mice at 8 to 10 weeks old were used in the studies. All animals were housed at 22–25°C with a 12 h light/dark cycle with food and water available ad libitum. The behavioral tests were conducted in the light phase of their light cycle. Mice were housed in five per cage and randomly assigned into experimental groups. All experimental protocols conformed to the National Institutes of Health Guide for the Care and Use of Laboratory Animals and were approved by the guidelines of the Institutional Animal Care and Use Committees at Xuzhou Medical University.

Mouse models of chronic pain

Chronic constriction injury of the sciatic nerve surgery. In accordance with the procedures described previously (Xu et al., 2015; Zhang et al., 2017), Chronic constriction injury (CCI) surgery was conducted to induce chronic neuropathic pain in mice under sodium pentobarbital (40 mg/kg, i.p.) anesthesia. In brief, in an aseptic condition, the left sciatic nerve at the mid-thigh level was exposed by blunt dissection. Three nonabsorbable 4-0 ligatures were placed around the nerve proximal to the trifurcation with 1.0 mm between each ligature. The ligatures were loosely tied until a short flick of the ipsilateral hindlimb was observed. Animals in the sham group received surgery identical to those described but without nerve ligation.

Complete Freund's adjuvant surgery. Complete Freund's adjuvant (CFA) (20 µl; F5881; Sigma-Aldrich) was intra-plantarly injected into the left hindpaw of the mouse to induce hyperalgesia of inflammatory pain (Xu et al., 2010; Singhmar et al., 2016). Sham groups received intraplantar injection of saline (20 µl).

Stereotaxic surgery and optic-fiber placement

Mice were anesthetized with 2% isoflurane and placed in a stereotaxic apparatus (RWD). Following sterilization, their skull was exposed by a scalpel incision. Microinjections were conducted with a Hamilton syringe needle (33 gauge) at a rate of 0.1 µl/min. The reagents or viruses were injected, respectively, into following: the VTA (anterior-posterior, −3.30 mm; lateral-medial, ±1.05 mm; dorsal-ventral, −4.60 mm, at a 7° angle), the dNAcMed (anterior-posterior, 1.60 mm; lateral-medial, ±0.6 mm; dorsal-ventral, −4.20 mm), the vNAcMed (anterior-posterior, 1.40 mm; lateral-medial, ±0.55 mm; dorsal-ventral, −4.70 mm), and the DRN (anterior-posterior, −4.50 mm; lateral-medial, 0 mm; dorsal-ventral, −3.00 mm). Following injection, the needle was held at the injection site for 5 min, then raised up by 0.05 mm and held for a further 5 min to allow the diffusion of the virus. The needle was then slowly withdrawn. Mice were maintained under a warm blanket until they fully recovered from anesthesia.

For optogenetics, an optic fiber (200 µm core, NA = 0.37, (Newdoon Inc.) held in a ferrule was implanted above the DRN (anterior-posterior, −4.50 mm; lateral-medial, 0 mm; dorsal-ventral, −2.80 mm). For a secure fixture of the implantable fiber to the skull, the skull was dried, and then dental cement was added between the base of the implantable fiber and the skull. For AAV surgeries, we carried out surgeries and then performed behavioral paradigm 3 weeks later when the AAV virus was expressed. For rabies tracing experiment, rabies virus was injected into the NAc 3 weeks after helper AAVs injection, and rabies virus was allowed to express for 7–12 d before starting immunohistochemistry analysis or behavioral paradigm. For retrograde labeling of VTA neurons projecting to the vNAcMed, the Lumafluor retrobeads (0.5 µl) were injected into the vNAcMed at the coordinates mentioned previously.

Viral constructs and drugs injection

The viruses used for neural tracing and neuronal manipulation were presented in Table 1. As in previously described concentrations (Felix-Ortiz et al., 2013; Noack et al., 2015), the glutamate AMPA receptor antagonist NBQX (22 mM, ab120045), and the NMDA receptor antagonist D-AP5 (38 mM, ab120003) were dissolved in saline. A volume of 0.5 µl was microinjected in behavioral studies. The Lumaflour (Lumafluor Inc.) was used for retrograde labeling of vNAcMed-projecting VTA neurons, shielded from light.

Optogenetic and chemogenetic manipulations

Blue light stimulation. In experiments with optogenetics applied, optic fiber implants were connected using an FC/PC adaptor to a 473 nm laser, and a stimulator (Newdoon Inc.) was used to generate blue light pulses. Electrical stimulation (20 Hz) of DR modulates pain responses (Andersen and Dafny, 1983; Qiao and Dafny, 1988). Therefore, 20 Hz optogenetic stimulation was used to drive action potentials in DRN cells in the present study. To test the effect of photoactivation of DRN-VTA^{DA}-NAc neurons, the pain threshold was determined paired with optical stimulation of blue light (5/10/20/50 Hz, eight pulses

Table 1. Virus strains used in this study

Item	Source	Identifier
rAAV-TH-NLS-Cre-WPRE-pA	BrainVTA	Cat#PT-0179
rAAV-Ef1α-DIO-His-EGFP-2a-TVA-WPRE-pA	BrainVTA	Cat#PT-0021
rAAV-Ef1α-DIO-RVG-WPRE-pA	BrainVTA	Cat#PT-0023
rAAV-CaMKIIα-Cre-WPRE-pA	BrainVTA	Cat#PT-0220
rAAV-THP2-Cre-WPRE-pA	BrainVTA	Cat#PT-0396
rAAV-hSyn-Cre-WPRE-pA	BrainVTA	Cat#PT-0136
rAAV-Ef1α-DIO-hChR2(H134R)-EYFP-WPRE-pA	BrainVTA	Cat#PT-0001
rAAV-Ef1α-DIO-hChR2(H134R)-mCherry-WPRE-pA	BrainVTA	Cat#PT-0002
rAAV-Ef1α-DIO-eNpHR3.0-EYFP-WPRE-pA	BrainVTA	Cat#PT-0006
rAAV-Ef1α-DIO-eNpHR3.0-mCherry-WPRE-pA	BrainVTA	Cat#PT-0007
rAAV-Ef1α-DIO-EYFP-WPRE-pA	BrainVTA	Cat#PT-0012
rAAV-Ef1α-DIO-mCherry-WPRE-pA	BrainVTA	Cat#PT-0013
rAAV-Ef1α-DIO-hM3D(Gq)-mCherry-WPRE-pA	BrainVTA	Cat#PT-0042
rAAV-Ef1α-DIO-hM4D(Gi)-mCherry-WPRE-pA	BrainVTA	Cat#PT-0043
rAAV-Ef1α-DIO-GCaMP6s-mCherry-WPRE-pA	BrainVTA	Cat#PT-0071
RV-ENVA-ΔG-dsRed	BrainVTA	Cat#R01002
RV-ENVA-ΔG-ChR2-dsRed	BrainVTA	Cat#R01012
RV-ENVA-ΔG-NpHR3.0-dsRed	BrainVTA	Cat#R02015

of 10 ms pulse-width, every 5 s, 10 mW, 473 nm). Two hours later, the pain threshold test was performed again with the light off. To observe the effect of repeated photoactivation of DRN-VTA^{DA}-NAc neurons, mice were subjected to a repeated (5 d, 20 min per day, eight pulses of 10 ms pulse-width, every 5 s, 10 mW, 473 nm) low-frequency (1 Hz) or high-frequency (20 Hz) optogenetic stimulation.

Yellow light stimulation. Optic fiber implants were connected using an FC/PC adaptor to a 589 nm laser, and a stimulator (Newdoon Inc.) was used to generate yellow light pulses. Mice were allowed to take a break of 30 min following the detection of the pain threshold baseline. For all in vivo behavioral experiments, mice were given a protocol of 15 s of yellow light on (10 mW, 589 nm) and then 5 s of light off during the thermal or mechanical pain threshold test. Approximately 2 h later, the pain threshold was measured again with light off.

Designer receptor exclusively activated by designer drugs. We used designer receptor exclusively activated by designer drugs (DREADDs) to manipulate the activities of hM3D(Gq)- or hM4D(Gi)-expressed neurons in a Cre-dependent manner (Lopez et al., 2016). For in vivo behavioral experiments, CNO (1 mg/kg, HY-17366, MedChemExpress) dissolved in DMSO was intraperitoneally injected 30 min before the pain threshold test to allow the medicine to work. Mice received another round of pain threshold determination 4 h after CNO was administrated.

Behavioral measurements

The following behavioral experiments were performed in a blinded manner and during daytime (light cycle), normally starting at 9 A.M. Animals were habituated to the testing environment daily for at least 1 h before testing. The room temperature and humidity remained stable for all experiments.

Thermal paw withdrawal latency test. To determine the thermal pain threshold, a thermal stimulation emitted by a thermal instrument (BEM-410A) was performed to detect paw withdrawal latency (PWL) of the left hindpaw. The basal paw withdrawal latency was adjusted to 9–15 s, with a cutoff of 20 s to prevent tissue damage. The detection was repeated three times at an interval of 5 min in a double-blinded manner. The mean of the PWLs was calculated and analyzed as the thermal pain threshold (Hargreaves et al., 1988; Liu et al., 2018).

Mechanical paw withdrawal threshold test. The von Frey test was used to detect the mechanical pain threshold. Mice were confined in boxes placed on an elevated metal mesh floor and a sequence of von Frey hairs was employed to perpendicularly stimulate the plantar surface of the left hindpaw with logarithmically increasing stiffness (0.16–2.00 g, Stoelting). Fifty percent of the paw withdrawal threshold (PWT) was calculated, conforming to the previously described up-down method (Han et al., 2016). The frequency response was measured by stimulating the hindpaw with a 0.16 or 0.4 g von Frey hair for 10 times, and the percentage withdrawal response was calculated as frequency (Taves et al., 2016).

Formalin test. Following an acclimation period of at least 30 min, 20 µl of 2.5% formalin dissolved in PBS was injected into the dorsal surface of the hindpaw with a 30 gauge needle. Animals received an intraperitoneal injection of DMSO or CNO (1 mg/kg) 10 min before the injection of formalin. The animals were returned to the plastic box immediately following the formalin injection. The time spent in licking paw was video-recorded and measured every 5 min up to 45 min after the injection. Additionally, the pain responses in acute (0–5 min) and inflammatory (15–45 min) phases were quantified.

Conditioned place preference procedures. To test whether inhibition of DRN-VTA neurons could induce conditioned place preference (CPP) in the chronic pain (CCI) model, we used a protocol as previously described procedures (King et al., 2009). All mice underwent 3 d of habituation in a two-compartment CPP chamber, which differed by both visual and tactile cues. On day 4, animal behavior was video-recorded for 15 min as the baseline. Baseline recordings generally showed a slight preference to one chamber. Mice that spent more than 80% of the total time in a chamber were not used for the experiments. On the conditioning days (day 5 to day 8), two training sessions were performed. In the morning session, mice were injected i.p. with DMSO 20 min before they were placed in their preferred CPP chamber for 1 h. In the afternoon sessions, the mice were injected i.p. with CNO (1 mg/kg, dissolved in DMSO) 20 min before they were placed in their nonpreferred chamber for 1 h. To test the CPP scores upon mechanical stimulation, each mouse was conditioned in the chamber and was stimulated with 0.16 g or 0.4 g von Frey filament every 2 min. The morning and afternoon sessions were separated by at least 4 h. The post-test was performed on day 9, and mice were placed in the CPP test box with access to both chambers and behavior was recorded for 15 min. CPP score was calculated by subtracting the time spent in the CNO-paired chamber during the pre-test from the time spent in the same chamber during the test.

Fiber photometry recording

Following viral injection, an optical fiber (125 µm OD, 0.37 numerical aperture (NA), Newdoon Inc.) was placed in a ceramic ferrule and inserted toward the DRN. Fiber photometry used the same fiber to both excite and record from GCaMPs in real-time. To record fluorescence signals, a laser beam was passed through a 488 nm laser (OBIS 488LS; Coherent), reflected off a dichroic mirror (MD498; Thorlabs), focused by an objective lens (Olympus), and coupled through a fiber collimation package (F240FC-A, Thorlabs) into a patch cable connected to the ferrule of the upright optic fiber implanted in the mouse via a ceramic sleeve (125 µm OD; Newdoon Inc.). The GCaMP6s fluorescence was bandpass filtered (MF525-39, Thorlabs) and collected by a photomultiplier tube (R3896, Hamamatsu). An amplifier (C7319, Hamamatsu) was used to convert the photomultiplier tube current output to voltage signals, which were further filtered through a low-pass filter (40 Hz cutoff; Brownlee 440). Analysis of the signal was performed with MATLAB software.

To analyze the responses to mechanical or thermal stimulation, a 30 s window around the stimulation point was analyzed. The baseline period was relative to stimulation onset (0 s), and the period from −10 s to 0 s was taken as the baseline Ca^{2+} value. The photometry signal F was converted to $\Delta F/F = (f - f_{baseline})/f_{baseline}$, where $f_{baseline}$ is the averaged baseline fluorescence signal. Each mouse received four times of stimulation with an interval of more than 2 min. The $\Delta F/F$ values of each mechanical stimulation were heat plotted for each mouse and averaged. $\Delta F/F$ values of mice within a group were then averaged and plotted with a shaded area indicating the SEM (Deng et al., 2020; Liu et al., 2022).

Patch-clamp recordings in acute brain slices

Experiments were performed on acute slices of mice brains (Stogsdill et al., 2017; Zhang et al., 2017). Mice were anesthetized with isoflurane to minimize stress and to obtain healthy brain slices. Murine brains were rapidly removed after decapitation and placed in high sucrose ice-cold oxygenated artificial cerebrospinal fluid (aCSF) containing the following (in mM): 254 sucrose, 3 KCl, 1.25 NaH_2PO_4, 2 $CaCl_2$, 2 $MgCl_2$, 24 $NaHCO_3$ and 10 D-glucose held at pH 7.4 by aeration with 95/5% O_2/CO_2. Acute coronal brain slices (250–300 μm) containing the DRN or the VTA were cut using a vibratome (VT1200S, Leica Biosystems) in cold sucrose aCSF saturated by 95/5% O_2/CO_2. Slices were maintained in holding chambers filled with aCSF containing the following (in mM): 128 NaCl, 3 KCl, 1.25 NaH_2PO_4, 2 $CaCl_2$, 2 $MgCl_2$, 24 $NaHCO_3$ and 10 D-glucose, pH 7.3, equilibrated with to 95/5% O_2/CO_2. The slices were allowed to recover at 32–34°C for 1 h and then maintained at room temperature.

Patch pipettes (4–6 MΩ) used for recordings were pulled from borosilicate capillaries (World Precision Instruments, Inc.) using a P-97 Flaming/Brown micropipette puller (Sutter Instrument Co.). For whole-cell recordings and cell-attached recordings, patch pipettes were filled with an internal solution containing the following (in mM): 115 potassium gluconate, 10 mM HEPES, 10 mM phosphocreatine, 1.5 mM $MgCl_2$, 20 mM KCl, 2 mM Mg-ATP and 0.5 mM GTP (pH 7.2, 285 mOsm). Cell-attached recordings were carried out using aCSF at ~32°C. The DRN neurons were discriminated by the fluorescence expression, and the DA neurons were identified by the fluorescence and then characterized by the electrophysiological properties (Krishnan et al., 2007): regular triphasic action potential waveforms, prolonged action potential duration, and low firing frequencies. To measure the intrinsic membrane properties of projection-specific DRN neurons, the spikes were induced by incremental increases of current injection (each step increase was 20 pA; range 0–200 pA). For recordings during optogenetic stimulation, the resting membrane potentials and action potentials were recorded using the Multiclamp 700B amplifier, and data acquisition was done in pClamp 10 (Molecular Devices). The series resistance was monitored during the experiments, and membrane currents and voltages were filtered at 2 kHz (Bessel filter). For ChR2 experiments, sustained and trains (1–50 Hz) of blue light were delivered to DRN neurons expressing ChR2 through an optical fiber (200 μm) coupled to a 473-nm laser that was placed within the bath and focused near the site of recording. For NpHR experiments, 15 s of yellow light were delivered to DRN neurons expressing NpHR through a 200 μm optic fiber attached to a 589 nm laser. The miniature excitatory postsynaptic currents EPSCs (mEPSCs) were recorded in the presence of 10 μM picrotoxin, 2 μM strychnine, and 0.5 μM tetrodotoxin (TTX). To record optic-evoked AMPAR and/or NMDAR EPSCs, patch pipettes were filled with the following (in mM): 140 $CsCH_3O_3S$, 20 HEPES, 5 TEA-Cl, 0.4 Cs-EGTA, 2.5 Mg-ATP, 0.5 GTP, and 1 QX-314 (pH 7.3). Presynaptic DRN afferents expressing ChR2 were activated, every 20 s, by blue light (473 nm, 5 mW, 5 ms) delivered through a 200 μm optic fiber, generated using the above-mentioned stimulator. Optic-evoked AMPAR EPSCs were optogenetically elicited at −70 mV, while NMDAR currents were elicited at a +50 mV holding potential. NMDAR amplitude was operationally defined as the amplitude of the current 40 ms after the onset of the evoked current (Huang et al., 2009). To determine the paired-pulse ratio, two EPSCs were evoked by a pair of blue light stimuli given at 50 ms intervals (Matthews et al., 2016). The paired-pulse ratio was presented as the ratio of the amplitude of the second synaptic response to the amplitude of the first synaptic response.

Immunohistochemistry

Mice were anesthetized using 2% isoflurane and were intracardially perfused with phosphate-buffered saline (PBS, 40 ml, PH 7.4) followed by 4% paraformaldehyde (PFA, 20 ml). Brains were subsequently separated and post-fixed in a 4% PFA solution at 4°C for 8–12 h. After post-fi xation, brains were washed with PBS and left in a 30% sucrose solution for 48–72 h. Successive frozen sections of brain tissue at 40 μm thick were prepared with a freezing microtome (VT1000S, Leica Microsystems). For immunofluorescent staining, sections were incubated with blocking buffer (3% bovine serum albumin in tris-buffered saline) for 2 h at room temperature, followed by washing in PBS for 3 × 5 min. A primary antibody (Table 2) was added at appropriate dilution in a staining solution (3% BSA and 0.2% Triton X-100 in TBS) and incubated overnight (4°C). Following washing in PBS for 3 × 5 min, sections were added by secondary antibody at appropriate dilution in a staining solution for 2 h at room temperature and then were washed in PBS for 3 × 5 min again. Finally, sections were mounted on slides, air-dried in darkness, and coverslipped. These sections were visualized by laser scanning confocal microscopy (LSM 880, Zeiss).

Table 2. Chemicals and antibodies used in this study

Item	Source	Identifier
Clozapine N-oxide	MedChemExpress	Cat#HY-17366
NBQX	Abcam	Cat#ab120045
D-AP5	Abcam	Cat#ab120003
Retrobeads Lumafluor	Lumafluor	N/A
Mouse monoclonal anti-TH antibody	Millipore	RRID:AB_2201528
Mouse monoclonal anti-CaMKIIα antibody	ThermoFisher	RRID:AB_325403
Rabbit monoclonal anti-c-fos antibody	Cell Signaling Technology	RRID:AB_2247211
Goat polyclonal anti-Serotonin antibody	Abcam	RRID:AB_1142794
Rabbit anti-glutamate antibody	Sigma-Aldrich	RRID:AB_259946
Donkey anti-mouse Alexa Fluor 488 antibody	ThermoFisher	RRID:AB_141607
Goat anti-mouse Alexa Fluor 405 antibody	ThermoFisher	RRID:AB_221604
Goat anti-mouse Alexa Fluor 594 antibody	ThermoFisher	RRID:AB_2534091
Donkey anti-goat Alexa Fluor 488 antibody	ThermoFisher	RRID:AB_2762838
Donkey anti-rabbit Alexa Fluor 488 antibody	ThermoFisher	RRID:AB_2762833

Experimental design and statistical analysis

The sample sizes were determined based on the literature of the field and our previous experience (King et al., 2009; Stogsdill et al., 2017; Zhang et al., 2017; Donnelly et al., 2021). No statistical methods were used to predetermine sample sizes. Each experiment was repeated in multiple animals (see relevant figure legends). The animals were randomly allocated to experimental groups in all experiments. Double-blind tests were adopted in all behavioral experiments. All data were expressed as mean ± standard error of the mean (SEM), as indicated in the figure legends. Statistical analysis was performed using GraphPad Prism (GraphPad Software, Inc.). Two experimental groups were compared using a two-tailed paired Student's *t* test or unpaired Student's *t* test, and three or more groups were compared using the one-way ANOVA or repeated measures one-way ANOVA with *post hoc* Tukey's tests for multiple comparisons. The comparison of behavioral data from different time points was made using a two-way repeated measures ANOVA, with *post hoc* Bonferroni's test, when appropriate. The criterion for statistical significance was $p < 0.05$.

Results

DRN glutamatergic neurons are activated in response to painful stimulation

DRN projection neurons are heterogeneous and include serotonergic, glutamatergic, GABAergic, and dopaminergic subpopulations (Vasudeva et al., 2011; Luo et al., 2015). The role of the DRN serotonin neurons in pain regulation is well known (Duggan and Griersmith, 1979; Cohen and Mao, 2014; De Gregorio et al., 2019). Therefore, we were interested in investigating the roles of DRN nonserotonin neurons in pain processing. The genetically encodable fluorescent calcium indicator, GCaMP6s, was utilized to enable real-time recording of fluctuations in neural activity (Gunaydin et al., 2014). We firstly expressed GCaMP6s in DRN glutamatergic neurons under the control of CaMKIIα promoter, which was recently used to label glutamatergic neurons in midbrain structures including the periaqueductal gray (PAG) and superior colliculus (Zhou et al., 2019; Huang et al., 2019a), and collected

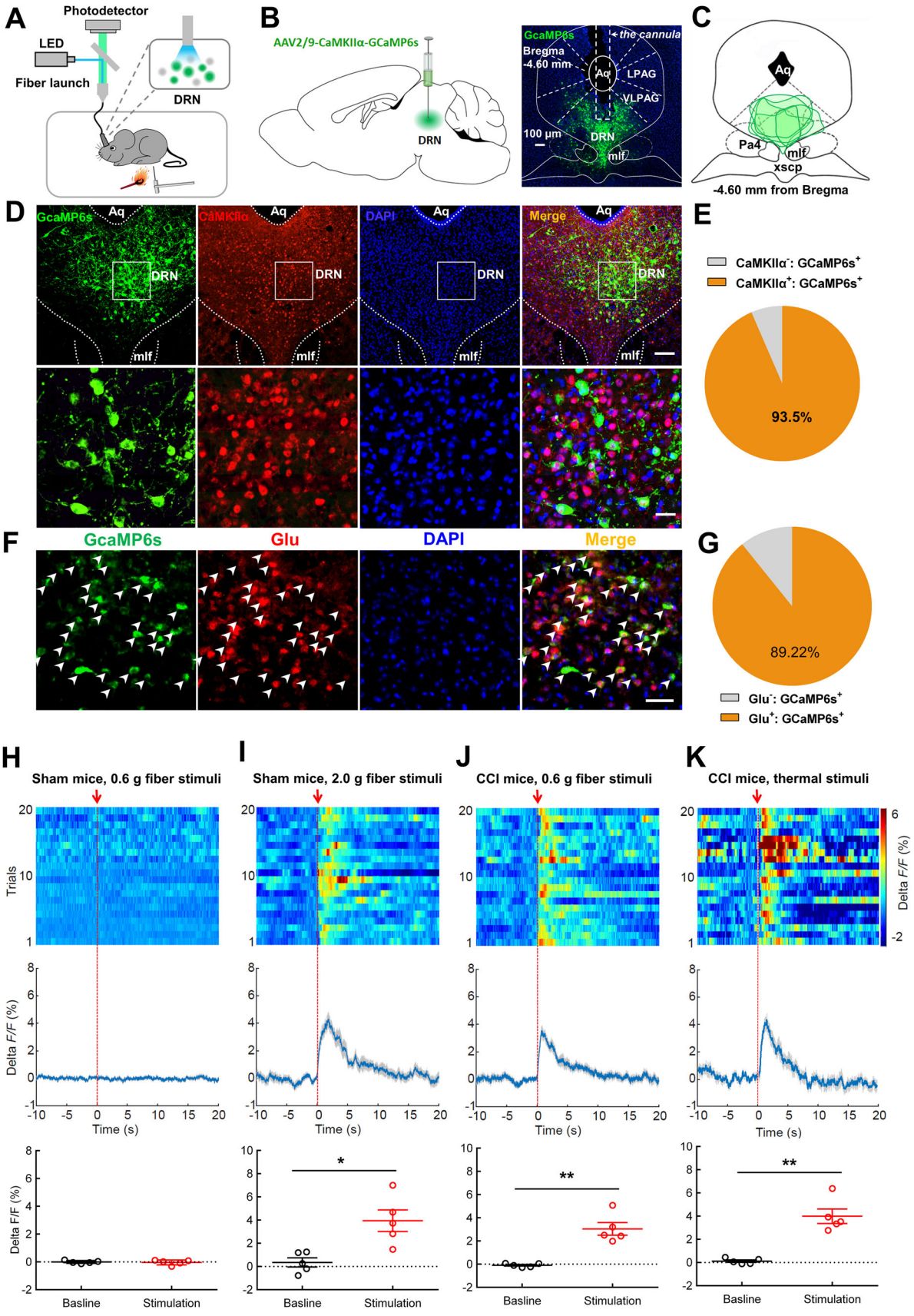

Figure 1. Continued.

GCaMP6s emission with optic fiber (Fig. 1*A–C*). We found that 93.5% of GCaMP6s-positive neurons co-labeled with CaMKIIα using immunohistochemistry (Fig. 1*D,E*). Furthermore, most of the GCaMP6s-positive neurons also expressed glutamate (Fig. 1*F,G*). Fiber photometry results showed that no significant change of fluorescence signal was observed in sham-operated mice in response to nonpainful 0.6 g von Frey filament stimulation on the hindpaw (Fig. 1*H*). Nevertheless, painful stimulation with 2.0 g von Frey filament notably increased the fluorescence signal in DRN neurons of sham-operated mice as compared to their basal activity (Fig. 1*I*). This effect was also found in CCI mice when they received 0.6 g von Frey filament stimulation (Fig. 1*J*), which was reliable to induce mechanical allodynia in these animals (Chen et al., 2015). Consistently, painful thermal stimulation triggered transient increases in calcium fluorescence in DRN glutamatergic cells (Fig. 1*K*). These data indicated activation of the DRN glutamatergic neurons upon painful stimulation.

We next investigated the calcium fluorescence signal in DRN DA neurons in response to painful stimulation. A mix (200 nl) of AAV expressing tyrosine hydroxylase (TH)-Cre- and Cre-dependent AAV-DIO-GCaMP6s was injected into the DRN (Fig. 2*A,B*). Interestingly, fiber photometry showed that neither mechanical stimulation in sham-operated mice nor CCI mice was able to change the fluorescence signal in DRN DA neurons (Fig. 2*C–E*). These data suggested that DRN DA neurons might not be involved in pain processing. We next injected AAV-DIO-GCaMP6s into the DRN of vesicular GABA transporter (Vgat)-Cre mice to examine the GABAergic neural activity in response to painful stimulation (Fig. 2*F,G*). Fiber photometry demonstrated that mechanical stimulation (0.6 or 2.0 g filament) did not change the fluorescence signal intensity in DRN GABA neurons (Fig. 2*H,I*). Additionally, the calcium activity was also not changed in CCI mice when they received 0.6 g filament stimulation (Fig. 2*J*). Taken together, these findings suggested that painful stimulation induced activation in DRN glutamatergic neurons.

Optogenetic activation of DRN glutamatergic neurons projecting to the VTA produces pain hypersensitivity

We aimed to investigate the DRN glutamatergic neuron's output circuitry that may mediate the pain responses. Following the injection of AAV-CaMKIIα-eYFP into the DRN, we observed dense eYFP$^+$ fibers in the VTA (Fig. 3), a brain region suggested being involved in the pathophysiology of pain perception (Brischoux et al., 2009; Zhang et al., 2017; Liu et al., 2018). To examine the functional importance of VTA-projecting DRN glutamatergic neurons in the regulation of pain sensation, GCaMP6s was expressed in these neurons through the Cre-dependent manner (Fig. 4*A,B*). We found that DRN-VTA CaMKIIα$^+$ neurons exhibited significant increases in calcium activity when mechanical painful stimulation was applied to the ipsilateral hindpaw of CCI mice (Fig. 4*C,D*). This effect was also seen in CCI mice when they received thermal painful stimulation in their ipsilateral hindpaw (Fig. 4*E,F*). These results suggested that VTA-projecting DRN glutamatergic neurons were activated in response to painful stimulation.

Next, we tested the effect of activating the DRN-VTA glutamatergic pathway on the pain threshold in sham-operated mice (Fig. 4*G*). Immunofluorescence staining and path-clamp recording confirmed functional ChR2 expression in DRN neurons (Fig. 4*H, I*). We delivered 473 nm light of 5 ms pulse-width at 20 Hz, a pattern used for DRN stimulation to promote behavioral changes (Liu et al., 2014; McDevitt et al., 2014), and found that optical activation of DRN-VTA glutamatergic neurons resulted in significant decreases in thermal paw withdrawal latency (Fig. 4*J*) and mechanical paw withdrawal threshold (Fig. 4*K*) in sham group mice. These data establish a causal role for DRN glutamatergic neurons in facilitating pain sensation.

DRN-VTA glutamatergic neurons are necessary for pain modulation

To determine whether DRN-VTA glutamatergic projection was necessary for pain processing, we investigated the effect of optogenetic inhibiting this pathway on the pain responses in CCI mice (Fig. 4*L*). Anatomical study and functional validation confirmed NpHR expression in DRN cells projecting to the VTA (Fig. 4*M–O*). Behavioral data revealed that optical inhibition of the DRN-VTA glutamatergic pathway attenuated the thermal hyperalgesia and mechanical allodynia in CCI mice (Fig. 4*P,Q*).

Additionally, the formalin test was performed to further evaluate the effect of suppressing DRN-VTA glutamatergic neurons on inflammatory pain with DREADD-based chemogenetics (Fig. 5*A*). With the validation of hM4Di expression in DRN neurons (Fig. 5*B–D*), mice were injected i.p. with DMSO or clozapine-N-oxide (CNO, 1 mg/kg, i.p.) 10 min before injection of formalin into the hindpaw (Zhou et al., 2018). We discovered that CNO injection reduced the second phase of the formalin test (Fig. 5*E,F*). Consistently, in the mouse model of neuropathic pain, chemogenetic inhibition of DRN-VTA glutamatergic neurons markedly relieved the thermal hyperalgesia and mechanical allodynia (Fig. 5*G–I*). Next, we investigated whether the DRN-VTA pathway identified was necessary for the affective aspect of chronic pain. Behavioral data showed that chemogenetic suppression of DRN-VTA glutamatergic neurons induced CPP in

←

Figure 1. Peripheral painful stimulation evokes calcium activity in DRN glutamatergic neurons. ***A***, Schematic for recording activity of GCaMP6s-expressing neurons in the DRN. ***B***, Experimental design showing viral injection (left panel) and the representative image displaying GCaMP6s expression and optic fiber placement (right panel). Scale, 50 µm. ***C***, GCaMP6s expression distributions at the DRN of mice used for photometry recording. ***D, E***, Confocal images (***D***) and quantification (***E***) showed that 93.5% of GCaMP6s-expressing DRN cells (green) were CaMKIIα-positive (red) ($n = 6$ sections from 5 mice). Scale, 100 µm (25 µm for insets). ***F***, Confocal images showing GCaMP6s (green) and glutamate (red) with white arrows indicating co-labeled neurons. ***G***, Quantitative data showed that the majority of DRN GCaMP6s-positive neurons expressed glutamate ($n = 6$ sections from 3 mice). Scale, 50 µm. ***H***, Response of DRN glutamatergic neurons following mechanical stimulation (von Frey, 0.6 g) in sham-operated mice (top, activity heatmap where each line corresponds to a single stimulation event, middle: average activity trace of 20 stimulation events; bottom, quantification of change in fluorescence in mice following exposure to stimulation). The red arrow indicates the time point at which stimulation occurred (paired *t* test, $t_4 = 0.2418$, $p = 0.8208$; $n = 5$ mice). ***I***, Response of DRN glutamatergic neurons following painful stimulation (von Frey, 2.0 g) in sham-operated mice. The red arrow indicates the time point at which stimulation occurred (paired *t* test, $t_4 = 4.237$, $^*p = 0.0133$, $n = 5$ mice). ***J***, Response of DRN glutamatergic neurons following mechanical stimulation (von Frey, 0.6 g) in CCI mice (top, activity heatmap where each line corresponds to a single stimulation event, middle: average activity trace of 20 stimulation events; bottom, quantification of change in fluorescence in mice following exposure to painful stimulation). The red arrow indicates the time point at which stimulation occurred (paired *t* test, $t_4 = 5.310$, $^{**}p = 0.006$, $n = 5$ mice). ***K***, Response of DRN glutamatergic neurons following painful thermal stimulation in CCI mice. The red arrow indicates the time point at which stimulation occurred (paired *t* test, $t_4 = 5.485$, $^{**}p = 0.0054$, $n = 5$ mice). Data are represented as mean ± SEM.

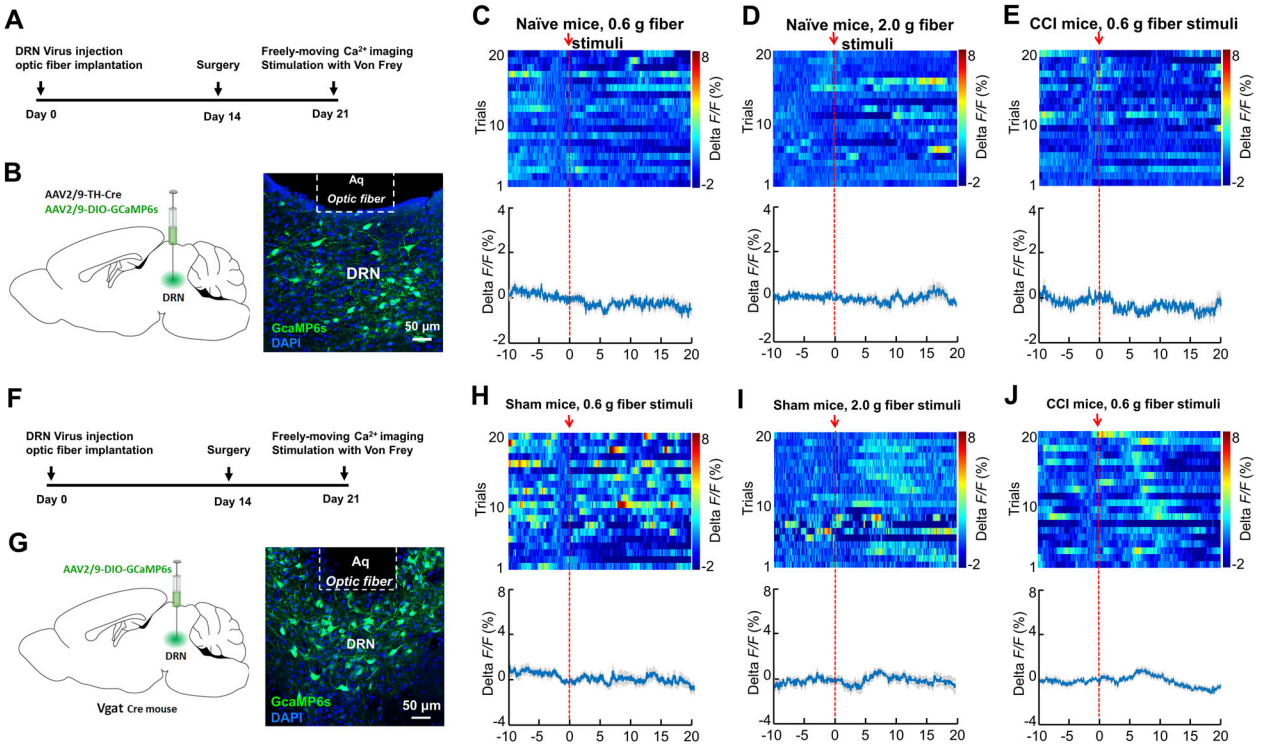

Figure 2. The Ca^{2+} activity of DRN dopaminergic and GABAergic neurons show insignificant response to painful stimulation. ***A***, Experimental design for GCaMP6s expression in DRN dopaminergic neurons and calcium imaging in freely moving mice. ***B***, Schematic showing viral injection (left panel). GCaMP6s was virally expressed and a GRIN lens was implanted to target the DRN region (right panel). Scale, 50 μm. ***C***, Response of DRN dopamine neurons following mechanical stimulation (von Frey, 0.6 g) in sham mice (top, activity heatmap where each line corresponds to a single stimulation event; bottom, average activity trace of 20 stimulation events). The red arrow indicates time point at which stimulation occurred ($n = 5$ mice). ***D***, Response of DRN dopamine neurons following painful stimulation (von Frey, 2.0 g) in sham mice (top, activity heatmap where each line corresponds to a single stimulation event; bottom, average activity trace of 20 stimulation events) ($n = 5$ mice). ***E***, Response of DRN dopamine neurons following mechanical stimulation (von Frey, 0.6 g) in CCI mice (top, activity heatmap where each line corresponds to a single stimulation event; bottom, average activity trace of 20 stimulation events) ($n = 5$ mice). ***F***, Experimental timeline. ***G***, Schematic showing viral injection in Vgat-Cre mice (left panel). GCaMP6s was virally expressed and a GRIN lens was implanted to target the DRN region (right panel). Scale, 50 μm. ***H***, Response of DRN GABAergic neurons following mechanical stimulation (von Frey, 0.6 g) in sham mice (top, activity heatmap where each line corresponds to a single stimulation event; bottom, average activity trace of 20 stimulation events). The red arrow indicates time point at which stimulation occurred ($n = 5$ mice). ***I***, Response of DRN GABAergic neurons following painful stimulation (von Frey, 2.0 g) in sham mice (top, activity heatmap where each line corresponds to a single stimulation event; bottom, average activity trace of 20 stimulation events) ($n = 5$ mice). ***J***, Response of DRN GABAergic neurons following mechanical stimulation (von Frey, 0.6 g) in CCI mice (top, activity heatmap where each line corresponds to a single stimulation event; bottom, average activity trace of 20 stimulation events) ($n = 5$ mice). Data are represented as mean ± SEM.

CCI mice (Fig. 5*J*,*K*). The CPP response is consistent with previous reports showing that relief of chronic pain alters preference responses in rodents (King et al., 2009; Lim et al., 2014). Furthermore, we found that the CPP scores were increased when sham mice were paired with CNO injection and mechanical stimulation with 0.16 g filament. However, the CPP scores were decreased when paired with CNO injection and mechanical stimulation with 0.4 g filament, which increased the withdrawal frequency in sham group mice (Fig. 5*L*,*M*). Collectively, these data suggested that DRN glutamatergic neurons projecting to the VTA are essential for the modulation of both sensory and affective components of pain.

DRN-VTA serotonergic neurons are not involved in pain processing

It was believed that a subpopulation of DRN glutamatergic neurons co-expressed rate-limiting enzymes for serotonin production (tryptophan hydroxylase; TPH) (Qi et al., 2014). Also, the DRN was the major source of serotonin in the forebrain (Baker et al., 1990; Jacobs and Azmitia, 1992), but it remained unclear whether VTA-projecting DRN serotonin neurons contributed to the regulation of pain sensation. We expressed GCaMP6s in DRN-VTA serotonin neurons under the control of a TPH2 promoter and tested the calcium fluorescence signal (Fig. 6*A*,*B*). Intriguingly, we found that the activity of DRN-VTA serotonin neurons did not exhibit notable change after applying mechanical stimulation (Fig. 6*C*–*E*), indicating that the DRN-VTA serotonin neurons did not significantly respond to painful stimulation.

We then assessed whether optogenetic manipulation of the DRN-VTA serotonin pathway was able to regulate pain sensation. The ChR2-mCherry or control virus was expressed in DRN-VTA serotonin neurons in a Cre-dependent manner (Fig. 6*F*). Immunofluorescence staining validated that the majority of $mCherry^{+}$ DRN neurons co-expressed serotonin (Fig. 6*G*, *H*). Whole-cell recording confirmed that the DRN-VTA serotonin neurons were reliably activated by optical stimulation (Fig. 6*I*). We optically activated these neurons and found that the pain threshold in sham mice was not changed (Fig. 6*J*). Furthermore, we revealed that optogenetic inhibition of the DRN-VTA serotonin pathway could not reverse thermal hyperalgesia and mechanical allodynia in CCI mice (Fig. 6*K*–*M*). Taken together, these data indicated that DRN-VTA serotonin neurons did not contribute to pain regulation.

Activation of DRN-VTA^{DA}-vNAcMed neurons in mice with neuropathic pain

Our data revealed that DRN-VTA glutamatergic neurons played an essential role in pain processing. How does the altered VTA

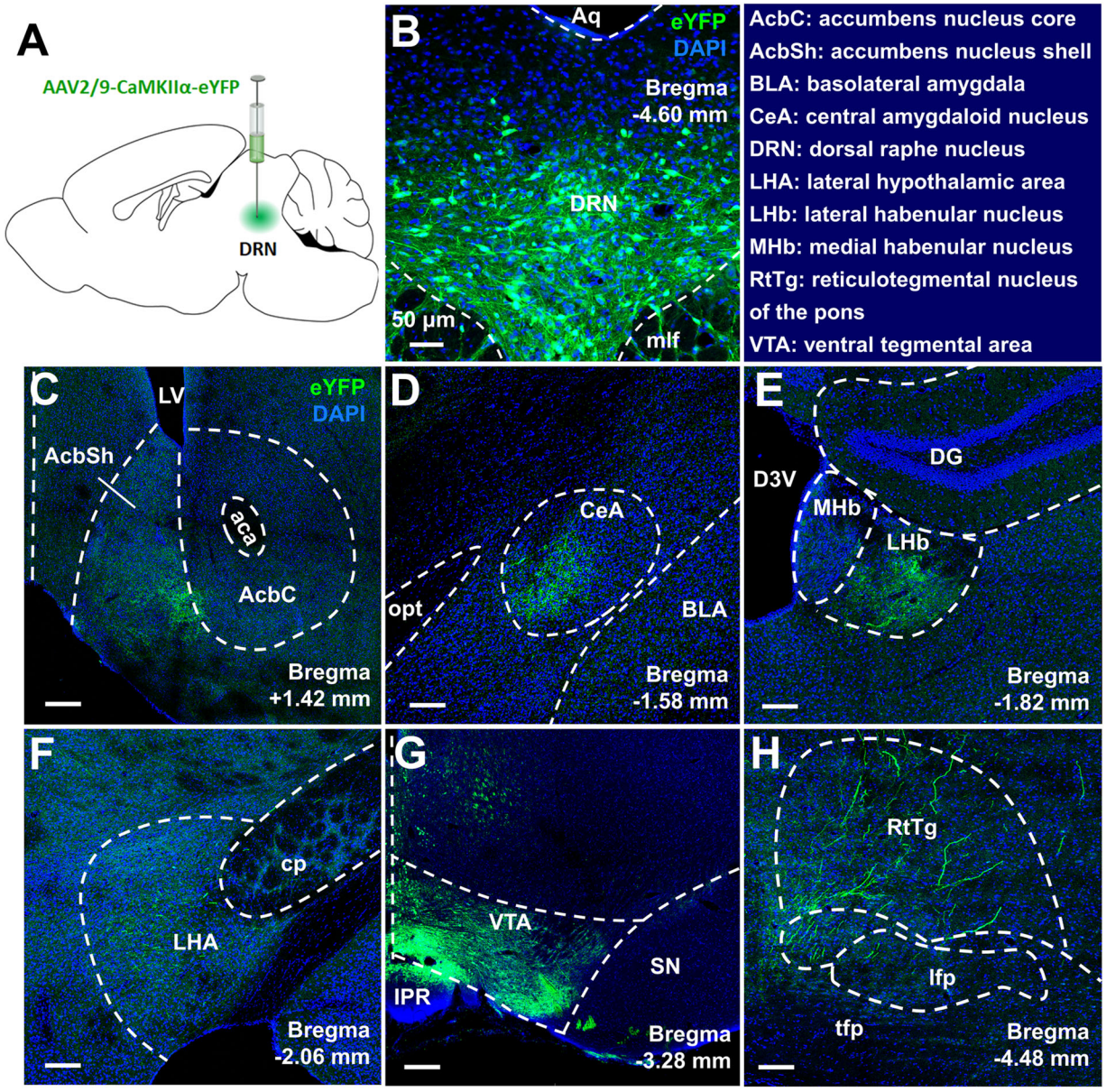

Figure 3. Viral tracking the outputs of DRN glutamatergic neurons. ***A***, The schematic showed an intra-DRN injection of AAV2/9-CaMKIIα-eYFP in wild-type mice. ***B***, Confocal images showing expression of eYFP in DRN neurons. Scale, 50 μm. ***C–H***, Coronal brain sections revealed that eYFP-positive terminals were expressed in the NAc (***C***), the central amygdaloid nucleus (CeA) (***D***), the lateral habenular nucleus (LHb) (***E***), the lateral hypothalamic area (LHA) (***F***), the VTA (***G***), and the reticulotegmental nucleus of the pons (RtTg) (***H***) following viral injection into the DRN. Scale, 150 μm.

output contribute to pain neuraxis? The shell region of NAc is an important hub that processes pain signals (Baliki et al., 2010; Baliki and Apkarian, 2015; Ren et al., 2016). The dopamine neurons that project to the NAc lateral shell were located in the lateral VTA, while neurons that project to the NAcMed were mainly located in the medial VTA (Lammel et al., 2011). When compared to the sham-operated mice, the in vitro firing rates were increased in VTA^{DA}-vNAcMed neurons, yet the firing activity in VTA^{DA}-dNAcMed neurons showed a decreasing tendency, in mice with neuropathic pain (Fig. 7*A–F*).

We subsequently aimed to characterize the anatomical and functional connections of the DRN and the mesolimbic dopamine pathway. To visualize presynaptic partners of VTA^{DA}-NAc neurons, we took advantage of the rabies-based tracing system (Watabe-Uchida et al., 2012; Deshpande et al., 2013; Beier et al., 2015). The helper viruses expressing RVG and TVA (Miyamichi et al., 2013) were infused into the VTA in mice that received an intra-vNAcMed injection of retrograde AAV-TH-Cre. Three weeks later, we injected a modified rabies virus (RV-EnvA-ΔG-DsRed) (Wall et al., 2010; Callaway and Luo, 2015) into the vNAcMed (Fig. 7*G*). Morphological data revealed that most of the EGFP-positive and DsRed-positive neurons in the VTA expressed TH (Fig. 7*H*). Consistent with previous results (Watabe-Uchida et al., 2012), we found that the VTA^{DA}-vNAcMed neurons received notable inputs from a cluster of $DsRed^{+}$ neurons within the DRN (Fig. 7*I*). Immunohistochemical classification demonstrated that the majority of $DsRed^{+}$ DRN neurons expressed CaMKIIα (Fig. 7*J*). Together, these results validated Cre-dependent and RV-based retrograde transsynaptic labeling of the DRN-VTA^{DA}-vNAcMed neurons.

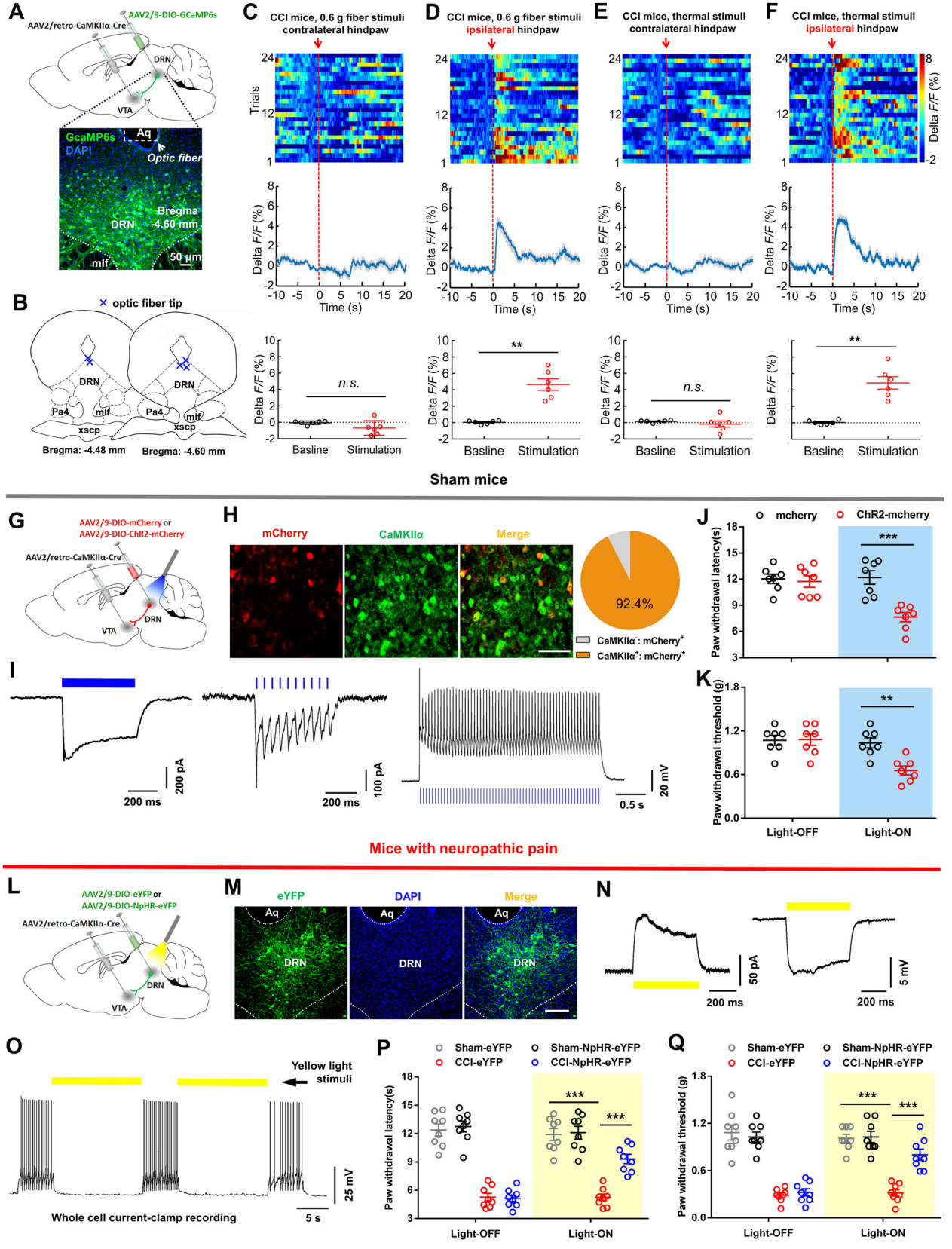

Figure 4. Continued.

We next used electrophysiological recording and c-Fos staining to investigate the activity of DRN neurons that synapse on VTA^{DA}-vNAcMed neurons in mice with neuropathic pain (Fig. 7*K*). Patch-clamp recording from DsRed^{+} DRN neurons in CCI mice showed a significantly higher firing rate as compared with controls (1.79 ± 0.18 Hz vs 3.68 ± 0.36 Hz) (Fig. 7*L*,*M*). We also found that the total numbers and percentages of c-Fos-expressing cells were increased in DsRed^{+} DRN neurons in CCI mice (Fig. 7*N–P*), which was consistent with previous studies reporting greater neural activity in rodents with chronic pain (Borges et al., 2013; Tache et al., 2014; Sagheddu et al., 2015). These results indicated that the activity of the DRN neurons innervating VTA^{DA}-vNAcMed neurons was increased after neuropathic pain.

DRN-VTA^{DA}-vNAcMed circuit is necessary and sufficient for pain regulation

We next studied whether DRN-VTA^{DA}-vNAcMed neurons were necessary for pain perception and investigated whether the pain regulatory roles were specific to this DRN-originated neural pathway. The ChR2-DsRed were expressed in DRN neurons innervating VTA^{DA}-vNAcMed neurons through rabies virus (Fig. 8*A*), and we tested the effect of activation of these neurons on pain threshold in sham mice. Behavioral data showed that optogenetic stimulation (5, 10, or 20 Hz, 473 nm) of DRN-VTA^{DA}-vNAcMed neurons reliably decreased the thermal (Fig. 8*B*) and mechanical (Fig. 8*C*) pain threshold, indicating that the activation of this pathway induced thermal and mechanical pain hypersensitivity.

To examine whether inhibiting this pathway rescued the pain responses in a mouse model of neuropathic pain, control rabies virus or one expressing NpHR was expressed in DRN-VTA^{DA}-vNAcMed neurons (Fig. 8*D*). Patch-clamp recording confirmed that the firing of these projection-specific DRN neurons was reliably inhibited by yellow light illumination (15 s on/5 s off, 589 nm) (Fig. 8*E*). Also, immunofluorescence staining validated a cluster of NpHR-DsRed-positive neurons within the DRN (Fig. 8*F*). Behavioral results showed that inhibition of DRN-VTA^{DA}-vNAcMed neurons attenuated the established thermal hyperalgesia and mechanical allodynia in CCI mice, whereas this effect was not observed in CCI mice expressing control rabies virus (Fig. 8*G*). Consistently, we found that optogenetic silencing of DRN-VTA^{DA}-vNAcMed neurons rescued pain hypersensitivity in a Complete Freund's adjuvant (CFA)-induced mouse model of inflammatory pain (Fig. 8*H*). These data suggested the necessary and sufficient roles of the DRN-VTA^{DA}-vNAcMed neurons for maintaining thermal hyperalgesia and mechanical allodynia in mice.

DRN neurons project directly to the NAc, and this DRN-NAc pathway is believed to participate in social interaction and decisions (Xu et al., 2017; Walsh et al., 2018). We thus wanted to know whether DRN neurons directly modulated pain via downstream NAc neurons. With validated hM3Dq expression in DRN-vNAcMed neurons, we found that chemogenetic activation of these neurons through CNO injection (i.p.,1 mg/kg) could not change pain threshold in sham mice (Fig. 9*A–D*). We then selectively expressed hM4Di in DRN-vNAcMed neurons and found that the chemogenetic silencing of these neurons was insufficient to rescue thermal hyperalgesia in CCI mice (Fig. 9*E–H*). Together, our findings indicated that DRN neurons predominately processed pain sensation via governing the VTA^{DA}-vNAcMed neurons but not through controlling the vNAcMed neurons directly.

Enhanced DRN excitatory synaptic transmission onto VTA^{DA}-vNAcMed neurons in neuropathic pain

We hypothesized that activation of DRN neurons in response to chronic pain increased the excitatory drive from the DRN to activate VTA^{DA}-vNAcMed neurons. To label the vNAcMed-projecting VTA DA neurons, retrograde AAV-TH-Cre and Cre-dependent AAV-DIO-eYFP were injected into the vNAcMed and VTA, respectively (Fig. 10*A*). Immunostaining validation showed that a substantial number of VTA^{DA}-vNAcMed neurons were targeted by this approach (Fig. 10*B*). Patch-clamp recording of miniature excitatory postsynaptic current (mEPSC) in eYFP^{+} VTA neurons in brain slices showed that the frequency and amplitude of mEPSC were significantly increased in CCI mice (Fig. 10*C–E*), indicating the involvement of excitatory synaptic transmission in pain modulation.

Next, we demonstrated how DRN glutamatergic neurons innervated VTA^{DA}-vNAcMed neurons, which neurotransmitters they released, and whether their activation was sufficient to elicit a

←

Figure 4. DRN-VTA glutamatergic neurons contribute to pain regulation. ***A***, Experimental design for calcium imaging in DRN-VTA neurons in freely moving mice. Scale, 50 µm. ***B***, The position of optic fiber tips (blue cross) in the DRN of mice used for photometry recording. ***C***, Response of DRN-VTA glutamatergic neurons following mechanical stimulation (von Frey, 0.6 g) in contralateral hindpaw of CCI mice (top, activity heatmap where each line corresponds to a single stimulation event; middle, average activity trace of 20 stimulation events; bottom, quantification of change in fluorescence in mice following exposure to mechanical stimulation). The red arrow indicates time point at which stimulation occurred (paired *t* test, $t_5 = 1.990$, $p = 0.1033$, $n = 6$ mice). ***D***, Response of DRN-VTA glutamatergic neurons following mechanical stimulation (von Frey, 0.6 g) in ipsilateral hindpaw of CCI mice (top, activity heatmap where each line corresponds to a single stimulation event; middle, average activity trace of 20 stimulation events; bottom, quantification of change in fluorescence in mice following mechanical stimulation). The red arrow indicates time point at which stimulation occurred (paired *t* test, $t_5 = 6.080$, $^{**}p = 0.0017$, $n = 6$ mice). ***E***, Response of DRN-VTA glutamatergic neurons following painful thermal stimulation in contralateral hindpaw of CCI mice. The red arrow indicates time point at which stimulation occurred (paired *t* test, $t_5 = 0.9764$, $p = 0.3737$, $n = 6$ mice). ***F***, Response of DRN-VTA glutamatergic neurons following painful thermal stimulation in ipsilateral hindpaw of CCI mice (paired *t* test, $t_5 = 6.676$, $^{**}p = 0.0011$, $n = 6$ mice). ***G***, Schematic showing viral injection. ***H***, Confocal images and quantification showed that 92.4% of mCherry-expressing DRN neurons were CaMKIIα-positive ($n = 3$ sections from 3 mice). Scale, 50 µm. ***I***, Whole-cell recording from ChR2-mCherry infected DRN neurons in slices showed that long duration (500 ms, left panel) or ten short bursts (20 Hz, middle panel) of blue light induced inward photocurrents and multiple short bursts (20 Hz, right panel) of blue light induced temporally precise spikes. ***J***, The effect of blue light illumination on thermal paw withdrawal latency in sham-operated mice expressing mCherry versus ChR2-mCherry (two-way repeated measures ANOVA, group × epoch interaction, $F_{1,12} = 21.68$, $p < 0.001$; *post hoc* Bonferroni's analysis, $^{***}p < 0.001$, $n = 7$ mice/group). ***K***, The effect of blue light illumination on mechanical paw withdrawal threshold in sham-operated mice (two-way repeated measures ANOVA, group × epoch interaction, $F_{1,12} = 9.674$, $p = 0.009$; *post hoc* Bonferroni's analysis, $^{**}p < 0.01$, $n = 7$ mice/group). ***L***, Schematic showing viral injection into the VTA and DRN. ***M***, Confocal images showing expression of NpHR-eYFP within the DRN. Scale, 100 µm. ***N***, Whole-cell recordings from NpHR-eYFP infected DRN neurons in brain slices showed that yellow light induced outward current (left panel) and hyperpolarized membrane potential (right panel). ***O***, Yellow light illumination inhibited the firing activity in an NpHR-eYFP-expressing DRN neuron. ***P***, Optogenetic inhibition of DRN-VTA pathway attenuated the thermal hyperalgesia in mice with neuropathic pain (two-way repeated measures ANOVA, group × epoch interaction, $F_{3,28} = 9.507$, $p < 0.001$; *post hoc* Bonferroni's analysis, $^{***}p < 0.001$, $n = 8$ mice/group). ***Q***, Optogenetic silencing of DRN-VTA glutamatergic neurons alleviated mechanical allodynia in CCI mice (Two-way repeated measures ANOVA, $F_{3,28} = 15.33$, $p < 0.001$; *post hoc* Bonferroni's analysis, $^{***}p < 0.001$, $n = 8$ mice/group). Data are represented as mean ± SEM.

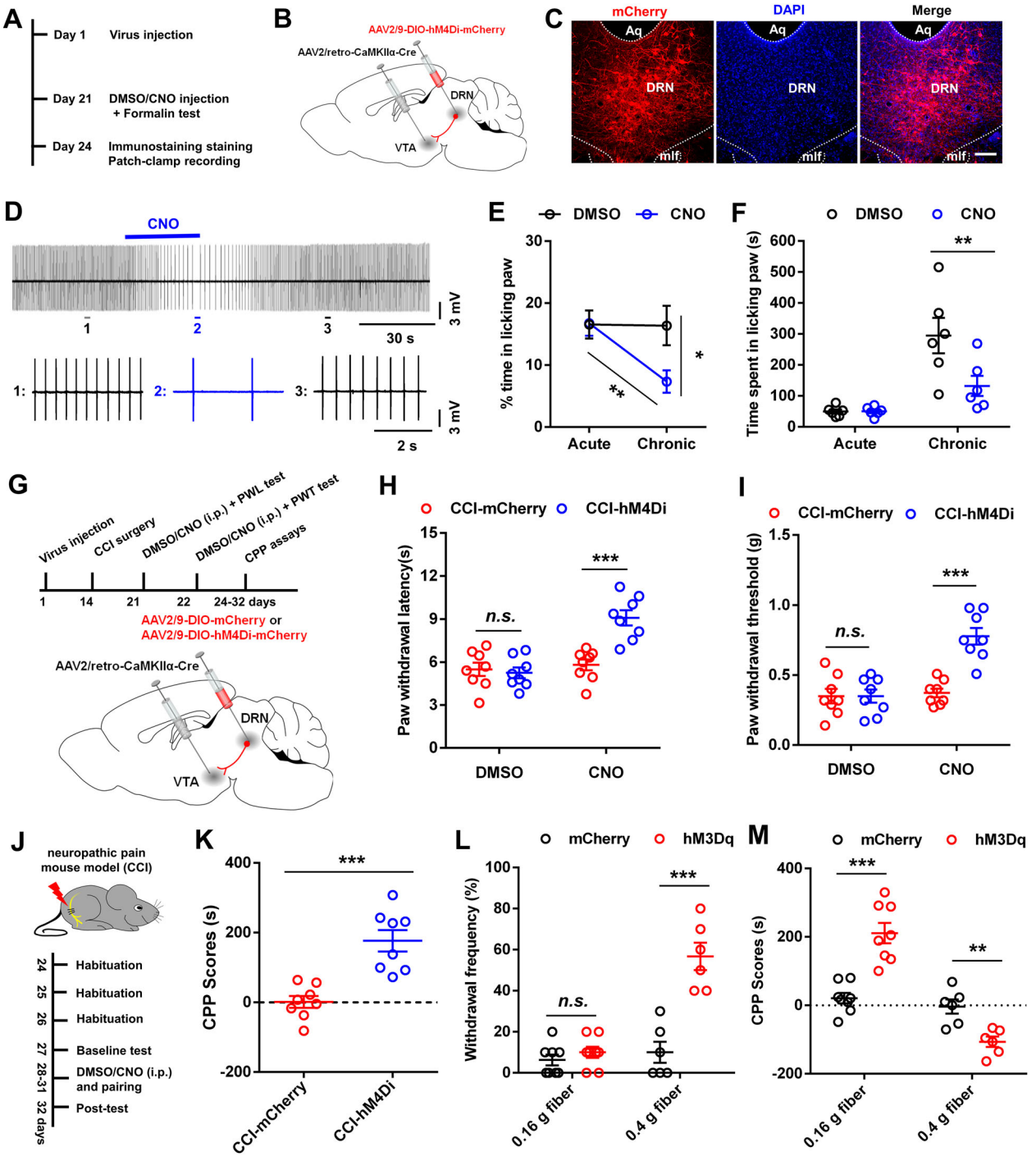

Figure 5. Effects of chemogenetic inhibition of DRN glutamatergic inputs into the VTA. ***A***, Experimental timeline for testing effects of chemogenetic suppressing DRN-VTA glutamatergic neurons on formalin-induced pain behavior. ***B***, Schematic showing AAV2/retro-CaMKIIα-Cre injected into the VTA and AAV-DIO-hM4Di-mCherry injected into the DRN. ***C***, Confocal images showing expression of hM4Di-mCherry in DRN neurons. Scale, 150 µm. ***D***, Representative traces showed that bath application of CNO (5 µm) reduced the firing activity in hM4Di-mCherry-expressing DRN neurons in the brain slice. ***E***, Percentage of time spent in paw licking during acute and inflammatory phases of formalin test (two-way repeated measures ANOVA, $F_{1,10} = 10.63$, $p = 0.009$; *post hoc* Bonferroni's analysis, $^{*}p < 0.05$, $^{**}p < 0.01$, $n = 6$ mice/group). ***F***, Time spent paw licking during the acute phase and the inflammatory phase of formalin test in hM4Di-expressed mice with an intraperitoneal injection of DMSO versus CNO (two-way repeated measures ANOVA, $F_{1,10} = 7.36$, $p = 0.0218$; *post hoc* Bonferroni's analysis, $^{**}p < 0.01$, $n = 6$ mice/group). ***G***, Experimental timeline (top panel) and schematic (bottom panel) showing viral injection, surgery, and behavioral tests. ***H***, Intraperitoneal injection of CNO (1 mg/kg) increased the thermal pain threshold in CCI mice expressing hM4Di-mCherry when compared to those expressing mCherry (two-way repeated measures ANOVA, $F_{1,14} = 24.48$, $p < 0.001$; *post hoc* Bonferroni's analysis, $^{***}p < 0.001$, $n = 8$ mice/group). ***I***, Chemogenetic inhibition of DRN-VTA glutamatergic neurons attenuated mechanical allodynia in CCI mice (two-way repeated measures ANOVA, $F_{1,14} = 45.68$, $p < 0.001$; *post hoc* Bonferroni's analysis, $^{***}p < 0.001$, $n = 8$ mice/group). ***J***, Experimental timeline. ***K***, Pairing with an intraperitoneal injection of CNO (1 mg/kg) induced CPP in CCI mice (Unpaired *t* test, $t = 5.007$, $^{***}p < 0.001$, $n = 8$ mice/group). ***L***, Intraperitoneal injection of CNO (1 mg/kg) increased the paw withdrawal frequency in sham mice during mechanical stimulation of the hindpaw with 0.4 g, but not 0.16 g, von Frey filament (Unpaired *t* test, $t = 5.534$, $^{***}p < 0.001$, $n = 6$–8 mice/group). ***M***, Pairing with CNO injection and mechanical stimulation of the hindpaw with 0.16 g von Frey fiber increased the CPP scores in sham mice. Pairing with CNO injection and stimulation of the hindpaw with 0.4 g fiber decreased the CPP scores in sham mice (for 0.16 g fiber, Unpaired *t* test, $t = 5.693$, $^{***}p < 0.001$, $n = 8$ mice/group; for 0.4 g fiber, Unpaired *t* test, $t = 3.989$, $^{**}p < 0.01$, $n = 6$ mice/group). Data are represented as mean ± SEM.

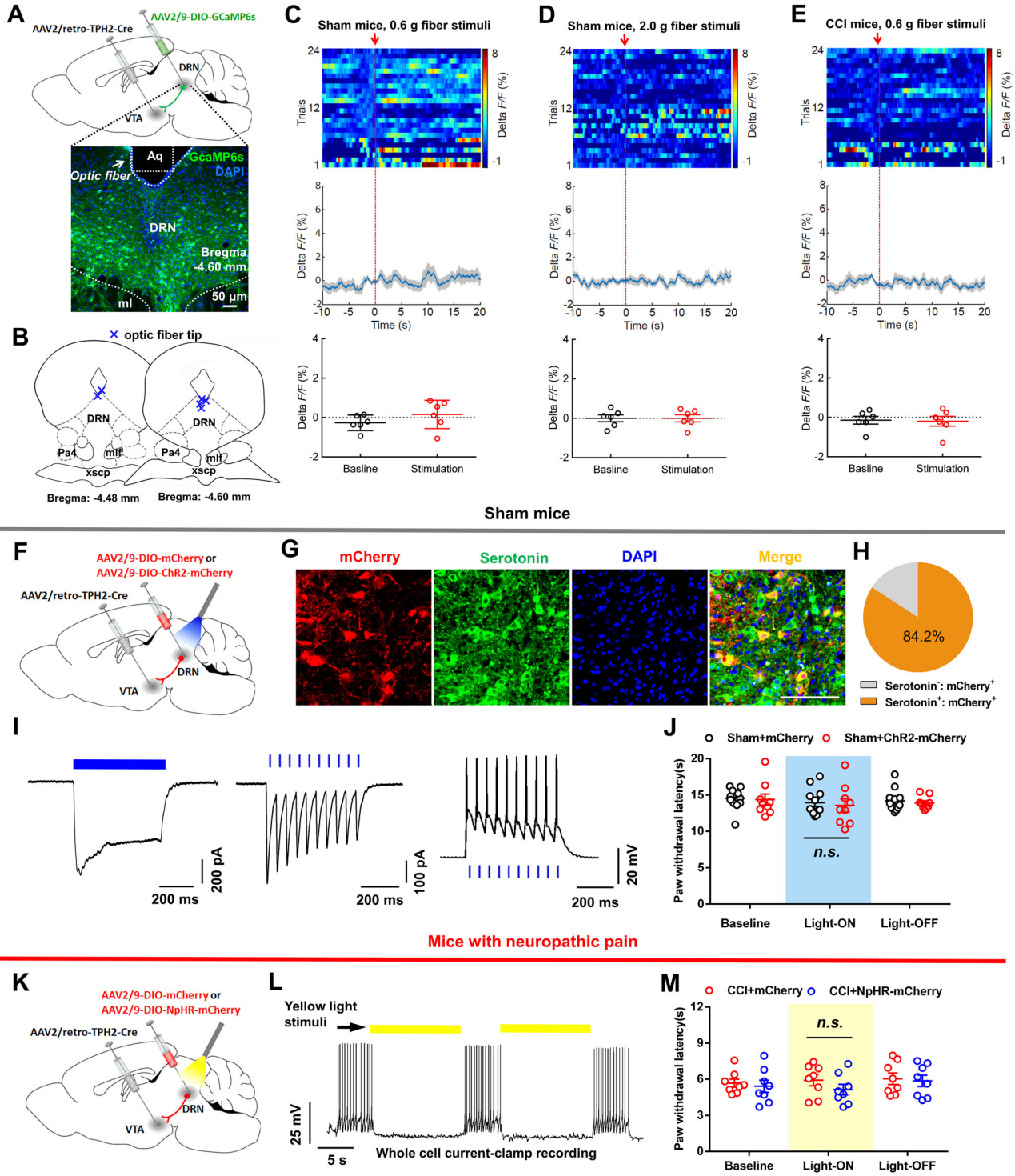

Figure 6. DRN-VTA serotonergic input plays insignificant roles in pain regulation. ***A***, Experimental design for expression of GCaMP6s in DRN-VTA serotonin neurons and calcium imaging in freely moving mice. Scale, 50 μm. ***B***, The position of optic fiber tips (blue cross) in the DRN of mice used for photometry recording. ***C***, Response of DRN-VTA serotonin neurons following mechanical stimulation (von Frey, 0.6 g) in sham-operated mice (top, activity heatmap where each line corresponds to a single stimulation event; middle, average activity trace of 24 stimulation events; bottom, quantification of change in fluorescence in mice following exposure to stimulation). The red arrow indicates time point at which stimulation occurred (paired *t* test, $t_5 = 1.141$, $p = 0.3055$, $n = 6$ mice). ***D***, Response of DRN-VTA serotonin neurons following painful stimulation (von Frey, 2.0 g) in sham-operated mice. The arrow indicates time point at which stimulation occurred (paired *t* test, $t_5 = 0.0164$, $p = 0.9876$, $n = 6$ mice). ***E***, Response of DRN-VTA serotonin neurons following mechanical stimulation (von Frey, 0.6 g) in CCI mice. The arrow indicates time point at which stimulation occurred (paired *t* test, $t_5 = 0.3216$, $p = 0.7608$, $n = 6$ mice). ***F***, Schematic showing viral injection into the DRN and VTA. ***G, H***, Confocal images (***G***) and quantification (***H***) showed that the majority of mCherry-expressing DRN cells were serotonin-positive ($n = 5$ sections from 3 mice). ***I***, In ChR2-mCherry infected DRN neurons, long duration (500 ms, left panel) or short bursts (20 Hz, 5 ms, middle panel) of blue light induced temporally precise inward photocurrents and short bursts (20 Hz, right panel) of blue light produced spikes. ***J***, There was no difference in thermal (left) and mechanical (right) pain thresholds between mCherry-expressed and ChR2-mCherry-expressed sham mice when they received blue light illumination (two-way repeated measures ANOVA, group × epoch interaction, left: $F_{1,\ 19} = 0.03038$, $p = 0.8635$; right: $F_{1,\ 19} = 0.5873$, $p = 0.4529$; $n = 9$, 12 mice/group). ***K***, Schematic showing viral expression of mCherry or NpHR-mCherry in DRN-VTA serotonin neurons. ***L***, The whole-cell recording revealed that yellow light illumination (15 s) of an NpHR-mCherry-positive DRN neuron reliably inhibits its firing activity. ***M***, Optic inhibition of DRN-VTA serotonin neurons could not change the thermal hyperalgesia (left) and mechanical allodynia (right) in CCI mice (two-way repeated measures ANOVA, group × epoch interaction, left: $F_{1,\ 14} = 0.3204$, $p = 0.5803$; right: $F_{1,\ 14} = 0.8597$, $p = 0.3695$; $n = 8$ mice/group). Data are represented as mean ± SEM.

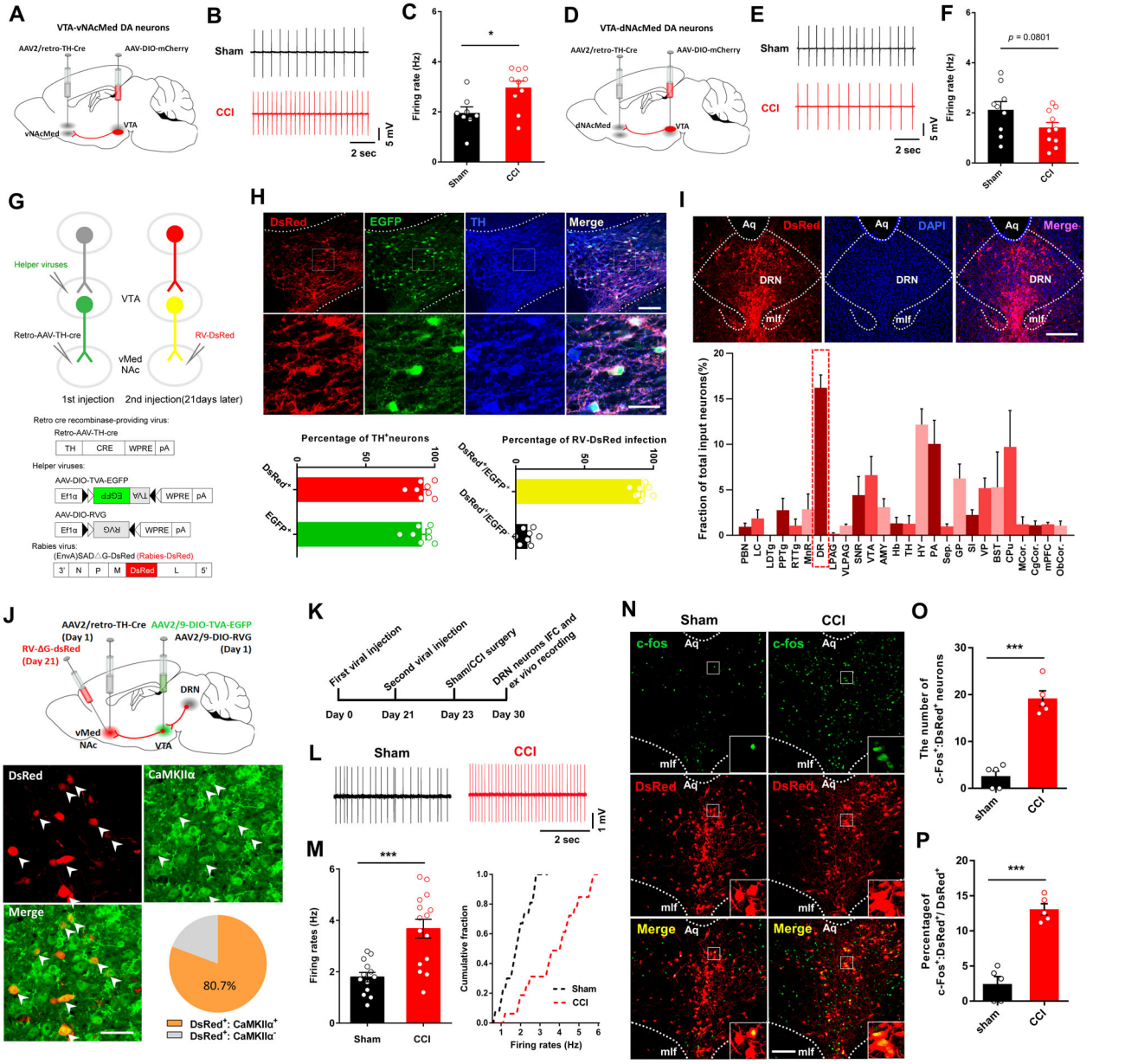

Figure 7. Neuropathic pain causes activation of DRN-VTA^{DA}-vNAcMed neurons. ***A***, Schematic of viral injection. ***B***, Sample traces recorded from VTA-vNAcMed neurons in VTA slices. ***C***, Firing rates of VTA-vNAcMed DA neurons from sham and CCI mice (two-tailed *t* test, $t_{16} = 2.800$, $^*p = 0.0128$; $n = 8$, 10 neurons/5 mice per group). ***D***, Anatomical injection sites for viruses. ***E***, Sample traces recorded from VTA-dNAcMed neurons in VTA slices. ***F***, Firing rates of VTA-dNAcMed DA neurons from sham and CCI mice (two-tailed *t* test, $t_{17} = 1.861$, $^*p = 0.0801$; $n = 9$, 10 neurons/5 mice per group). ***G***, Schematic for labeling presynaptic partners of VTA^{DA}-vNAcMed neurons using the rabies-based tracing tools. ***H***, Confocal images (top panel) and quantification (bottom panel) showing co-expression of DsRed and EGFP in TH-positive cells ($n = 2$ sections from $n = 4$ mice). The insets indicated an enlarged box. Scale, 50 μm (20 μm for insets). ***I***, Whole-brain input data to the VTA^{DA}-vNAcMed neurons (bottom panel) and representative DRN neurons (top panel) are defined by transsynaptic labeling. Brain region is plotted on the *x*-axis, and percentage of total inputs is on the *y*-axis ($n = 4$). Scale, 200 μm. ***J***, Diagrams of the injection sites for rabies labeling of DRN-VTA^{DA}-vNAcMed neurons (top panel). Representative images and quantification showed the immunofluorescent staining signals in the DRN (green for CaMKIIα and red for DsRed) with white arrows indicating co-labeled neurons ($n = 4$ sections from 4 mice). Scale, 25 μm. ***K***, Experimental paradigm for testing the neural activity of DRN-VTA^{DA}-vNAcMed neurons in mice with neuropathic pain. ***L***, Sample traces showing firing activity of DRN-VTA^{DA}-vNAcMed neurons from CCI mice and sham controls. ***M***, Comparison (left panel) and cumulative probability distributions (right panel) of firing rate in DRN-VTA^{DA}-vNAcMed neurons from two groups of mice ($t_{26} = 4.417$, $^{***}p < 0.001$; two-tailed *t* test, $n = 13$, 15). ***N***, Confocal images showing DsRed (Red) and c-Fos (Green) in DRN slices from sham and CCI mice. The insets indicated DRN neurons co-expressing DsRed and c-Fos. Scale, 80 μm. ***O***, Total numbers of DRN neurons co-expressing DsRed and c-Fos ($t_8 = 8.630$, $^{***}p < 0.001$; two-tailed *t* test, $n = 5$ mice/group). ***P***, Percentages of c-Fos-expressing neurons in DsRed$^+$ DRN neurons ($t_8 = 8.084$, $^{***}p < 0.001$; two-tailed *t*-test, $n = 5$ mice/group).

notable postsynaptic effect. The VTA^{DA}-vNAcMed neurons were labeled through injection of red retrobeads into the vNAcMed, and ChR2-eYFP was expressed in the DRN-VTA CaMKIIα$^+$ neurons in a Cre-dependent manner (Fig. 10*F*). We found that 91.1% of retrobeads$^+$ neurons co-labeled with TH (Fig. 10*G*,*H*), which is consistent with the overlap reported in previous studies (Chaudhury et al., 2013; Liu et al., 2018). Furthermore, the retrobeads$^+$ neurons were surrounded by dense terminals of VTA-projecting eYFP$^+$ DRN neurons (Fig. 10*G*). We next prepared VTA slices and optogenetic stimulation of ChR2-expressing DRN neural terminals elicited AMPAR-mediated EPSC in retrobeads$^+$ neurons (Fig. 10*I*–*K*). Moreover, the EPSC could be blocked by TTX and restored in the presence of 4-aminopyridine (4-AP) (Fig. 10*L*), suggesting a monosynaptic glutamate release

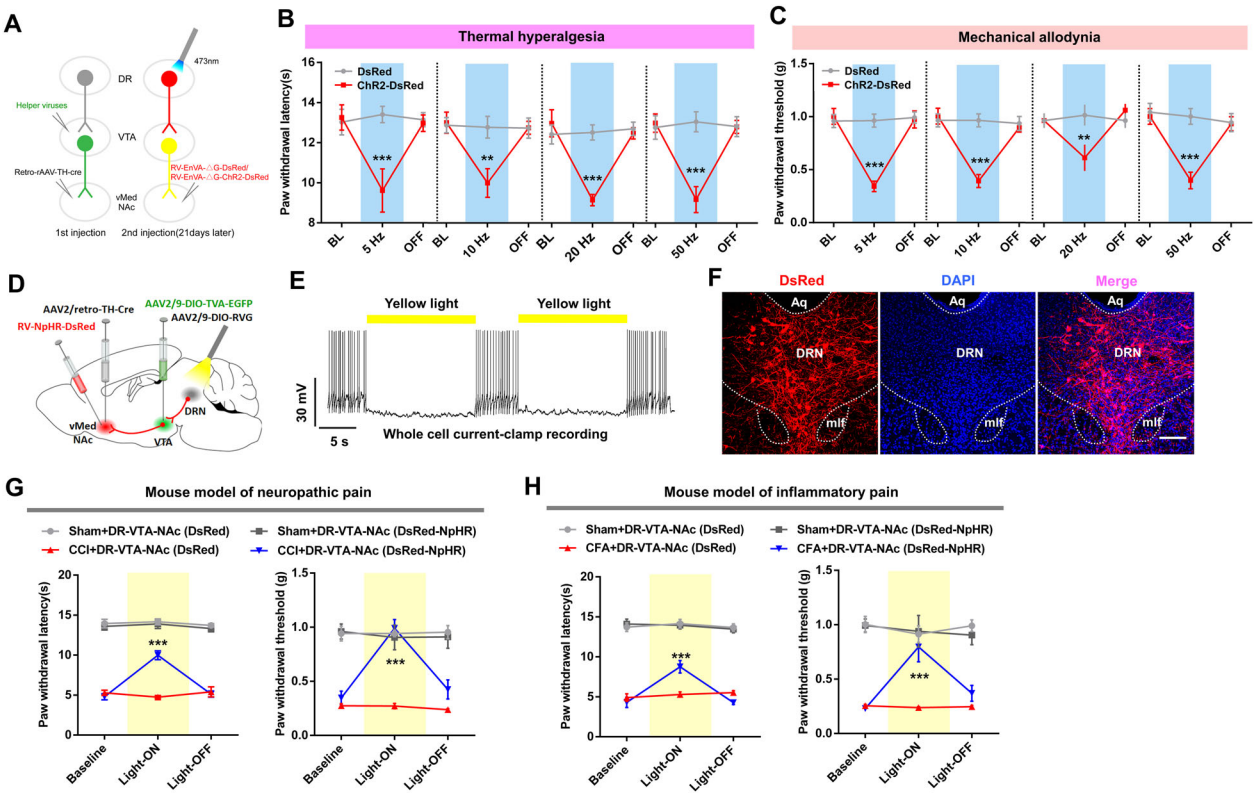

Figure 8. Regulation of pain behavior by DRN-VTA^{DA}-vNAcMed neurons. ***A***, Schematic for optogenetic activation of DRN-VTA^{DA}-vNAcMed neurons in sham mice. ***B***, Optogenetic stimulation (5, 10, or 20 Hz) of DRN-VTA^{DA}-vNAcMed neurons decreased the thermal pain threshold in sham-operated mice (two-way repeated measures ANOVA, $F_{2,28} = 6.856$, $p = 0.0038$ for 5 Hz; $F_{2,28} = 8.471$, $p = 0.0013$ for 10 Hz; and $F_{2,28} = 16.87$, $p < 0.001$ for 20 Hz; *post hoc* Bonferroni's test, $^{**}p < 0.01$, $^{***}p < 0.001$, $n = 8$ mice/group). ***C***, Photoactivation of DRN-VTA^{DA}-vNAcMed neurons induced a notable decrement in mechanical pain threshold in sham-operated mice (two-way repeated measures ANOVA, $F_{2,28} = 13.76$, $p < 0.001$ for 5 Hz; $F_{2,28} = 25.84$, $p < 0.001$ for 10 Hz; and $F_{2,28} = 6.484$, $p = 0.0049$ for 20 Hz; *post hoc* Bonferroni's test, $^{**}p < 0.01$, $^{***}p < 0.001$, $n = 8$ mice/group). ***D***, Schematic showing RV and AAVs injection to specifically expressed NpHR in DRN-VTA^{DA}-vNAcMed neurons. ***E***, Yellow light illumination inhibited spiking in DsRed-positive DRN neurons. ***F***, Confocal images showing the DRN neurons labeled with RV-EnvA-NpHR-DsRed. Scale, 150 µm. ***G***, NpHR-DsRed-expressing CCI mice showed significant increments in thermal PWLs (left panel) and mechanical PWTs (right panel) when compared with DsRed-expressing CCI mice during the illumination epoch (two-way repeated measures ANOVA, group × epoch interaction, $F_{6,52} = 17.50$, $p < 0.001$ for thermal pain threshold assays; group × epoch interaction, $F_{6,52} = 8.322$, $p < 0.001$ for mechanical pain threshold tests; *post hoc* Bonferroni's analysis, $^{***}p < 0.001$, $n = 7$, 8 mice). ***H***, During yellow light illumination, CFA mice with DRN-VTA^{DA}-vNAcMed neurons expressing NpHR-DsRed revealed prolonged thermal PWLs and increased mechanical PWTs when compared with those expressing DsRed (two-way repeated measures ANOVA, group × epoch interaction, $F_{6,50} = 9.337$, $p < 0.001$ for thermal pain threshold; group × epoch interaction, $F_{6,50} = 5.586$, $p < 0.001$ for mechanical pain threshold; *post hoc* Bonferroni's analysis, $^{***}p < 0.001$, $n = 7$, 8 mice). Data are represented as mean ± SEM.

in VTA^{DA}-vNAcMed neurons (Petreanu et al., 2007; Felix-Ortiz et al., 2013). Taken together, these data demonstrated that optogenetic stimulation of DRN CaMKIIα^{+} neurons triggered rapid glutamate release in VTA^{DA}-vNAcMed neurons.

We next investigated whether presynaptic DRN glutamatergic neurons contributed to the enhanced excitatory synaptic transmission observed in the VTA from CCI mice. The ChR2 was virally expressed in DRN-VTA glutamatergic neurons, and VTA^{DA}-vNAcMed neurons were labeled with retrobeads (Fig. 10*M*). We found that the amplitude of EPSC in VTA^{DA}-vNAcMed neurons evoked by blue light stimulation was increased in CCI mice (Fig. 10*N*). The paired-pulse ratio of light-evoked EPSC, which was inversely related to presynaptic neurotransmitter release (Zhang and Pan, 2010; Di Castro et al., 2016), was reduced in CCI mice (Fig. 10*O*). These data indicated increased presynaptic glutamate release in mice with chronic pain. Furthermore, the ratio of light-evoked AMPAR- and NMDAR-mediated EPSC (AMPA/NMDA ratio) in VTA^{DA}-vNAcMed neurons was significantly increased in CCI mice (Fig. 10*P*), suggesting a postsynaptic potentiation at DRN-VTA synapses in mice with neuropathic pain. Overall, these results suggest nerve injury potentiates synaptic transmission via mechanisms that likely involve an increase in presynaptic transmitter release probability and responsiveness of postsynaptic AMPARs.

Repeated activation of DRN-VTA^{DA}-vNAcMed pathway in sham mice mimics synaptic, cellular, and behavioral phenotypes induced by chronic pain

We further investigated the causal link between the potentiation of excitatory synaptic transmission and the pronociceptive roles of the DRN-VTA^{DA}-vNAcMed pathway. We used rabies tracing tools to express ChR2-DsRed in DRN-VTA^{DA}-vNAcMed neurons and repeatedly delivered blue light (1 Hz or 20 Hz, 473 nm) to these neurons in sham mice (Fig. 11*A*). Blue light reliably induced photocurrents in DRN DsRed^{+} neurons (Fig. 11*B*). Behavioral data revealed that the pain threshold in ChR2-expressing mice was similar to DsRed-expressing controls following repeated 1 Hz illumination of DRN-VTA^{DA}-vNAcMed neurons (Fig. 11*C*). However, repeated 20 Hz optic stimulation of these neurons significantly reduced the paw thresholds in sham mice, and this effect lasted for at least 24 h, indicating a persistent pain-like behavior (Fig. 11*D*).

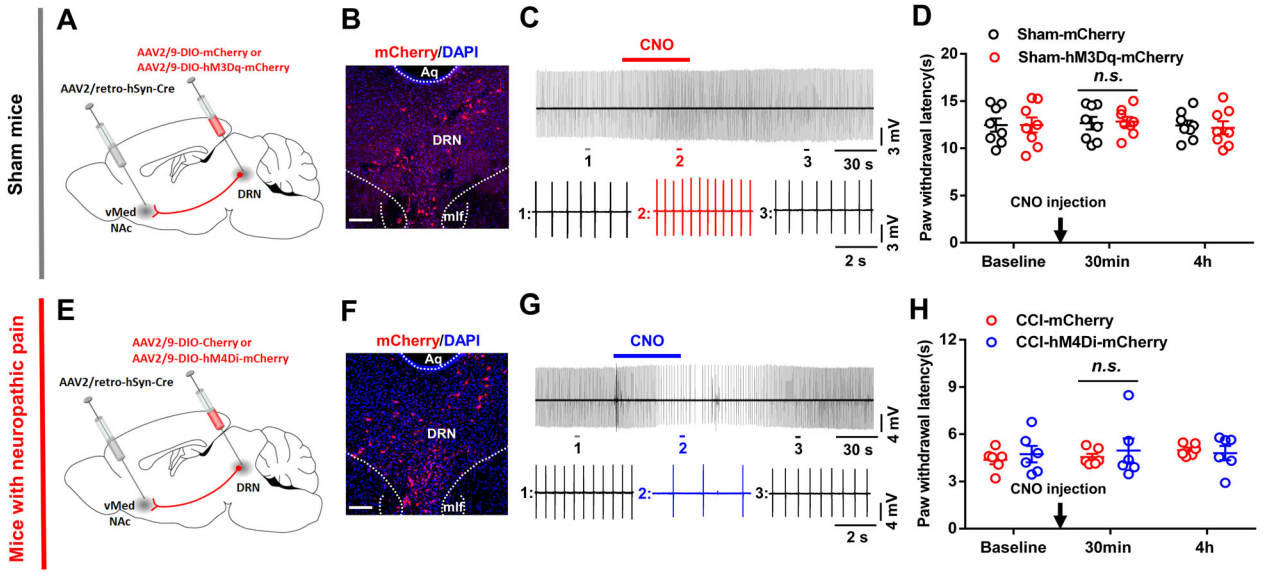

Figure 9. The effects of optogenetic manipulation of DRN-vNAcMed pathway on the pain threshold in mice. ***A***, Schematic showing AAV2/retro-hSyn-Cre injected into the vNAcMed and AAV-DIO-mCherry or AAV-DIO-hM3Dq-mCherry injected into the DRN. ***B***, Confocal images revealing hM3Dq-mCherry expression in DRN. Scale, 150 µm. ***C***, Representative traces showing bath application of CNO (5 µM) increased the firing activity of a neuron expressing hM3Dq-mCherry in the DRN slice. ***D***, There was no significant difference in thermal pain threshold between mCherry- and hM3Dq-mCherry-expressing sham mice when they received CNO injection (1 mg/kg, i.p.) (two-way repeated measures ANOVA, $p > 0.05$, $n = 8$ mice/group). ***E***, Schematic showing viral injection into the vNAcMed and the DRN. ***F***, Confocal images showing hM4Di-mCherry expression in the DRN. Scale, 150 µm. ***G***, Representative traces showing the changes in the firing activity of a hM4Di-mCherry-expressing DRN neuron after bath application of CNO (5 µM). ***H***, CNO injection (1 mg/kg, i.p.) could not change the pain threshold in CCI mice with DRN-vNAcMed neurons expressing hM4Di-mCherry when compared with those expressing mCherry (two-way repeated measures ANOVA, $p > 0.05$, $n = 6$ mice/group). Data are represented as mean ± SEM.

To further investigate the mechanisms underlying this facilitatory effect on pain sensation, we examined whether activation of DRN-VTA^{DA}-vNAcMed neurons induced downstream changes in VTA^{DA}-vNAcMed neurons (Fig. 11*E*). Our data demonstrated that repeated optical stimulation of DRN-VTA^{DA}-vNAcMed neurons increased the firing rate of DsRed^{+}/EGFP^{+} VTA^{DA}-vNAcMed neurons (3.38 ± 0.31 Hz), with no change observed in the firing activity of DsRed^{-}/EGFP^{+} VTA^{DA}-vNAcMed neurons (2.07 ± 0.26 Hz) (Fig. 11*F*,*G*). These findings were consistent with studies reporting enhanced firing activity of VTA^{DA}-NAc neurons in mice with pain hypersensitivity (Brischoux et al., 2009; Zhang et al., 2017; Liu et al., 2018). We also found that both frequency and amplitude of mEPSC were increased in DsRed^{+}/EGFP^{+} VTA neurons from mice received repeated optical activation (Fig. 11*H–J*).

Finally, to test which glutamate receptors in VTA mediate the algesic effect of DRN-VTA^{DA}-vNAcMed neurons, optical stimulation was delivered to DRN neurons of sham mice with an intra-VTA injection of AMPA receptor antagonist (NBQX) and NMDA receptor antagonist (D-AP5) (Fig. 12*A*,*B*). We found that intra-VTA infusion of either NBQX or a cocktail of NBQX and D-AP5, but not D-AP5, reversed the optical stimulation-induced pain-like behavior (Fig. 12*C–E*), indicating AMPA receptor was necessary for the algesic effects of DRN-VTA^{DA}-vNAcMed neurons. Collectively, these results demonstrated that repeated activation of DRN-VTA^{DA}-vNAcMed neurons induced firing adaptation and synaptic plasticity in VTA^{DA}-vNAcMed neurons and produced persistent pain-like behaviors.

Discussion

In this study, we utilized rabies-based transsynaptic tracing and cell-type-specific manipulation to demonstrate previously unknown roles of a subset of DRN glutamatergic neurons in pain facilitation. We also identified the functional importance of downstream VTA^{DA}-vNAcMed neurons in the procedure. The following part discussed the implications of these findings.

The role of DRN in pain regulation has been the subject of investigation for several decades, and it has been classically recognized as a nucleus suppressing pain sensation through a descending pain inhibitory pathway (Segal, 1979; Andersen and Dafny, 1983; Li et al., 2016). For example, in some early-stage studies, electrical stimulation of the DRN nonselectively reduced the responses of dorsal horn neurons to painful stimulation (Duggan and Griersmith, 1979) and produced an analgesic effect (Reynolds, 1969; Mayer and Price, 1976). The knock-out of lynx1, an inhibitory modulator of nAChRs, in mouse DRN is also thought to activate the neurons thereby and consequently augment the analgesic effect of nicotine (Nissen et al., 2018). Here, we provided evidence indicating an algesic property of DRN glutamatergic neurons.

The diverse subpopulations of DRN neurons are functionally heterogeneous (Vong et al., 2011; Liu et al., 2014; McDevitt et al., 2014; Matthews et al., 2016). The serotonin neurons are generally considered to be antagonistic to pain (Segal, 1979; Singh et al., 2017; De Gregorio et al., 2019). Previous reports indicate that activation of PAG/DRN DA neurons promotes analgesic effects (Li et al., 2016; Yu et al., 2021), which seems inconsistent with the insignificant changes in calcium activity of DRN DA neurons in our study. The prior studies focused on both DRN and adjacent PAG; however, the smaller volume of virus we infused (200 nl) that allowed fiber photometry could be relatively confined to the DRN region. Moreover, Cre-inducible expression systems likely depend on both the levels of Cre recombinase and the number of transgenes undergoing recombination, making it difficult to compare the results in the present study using the AAV-TH-Cre virus and previous reports applying TH-Cre

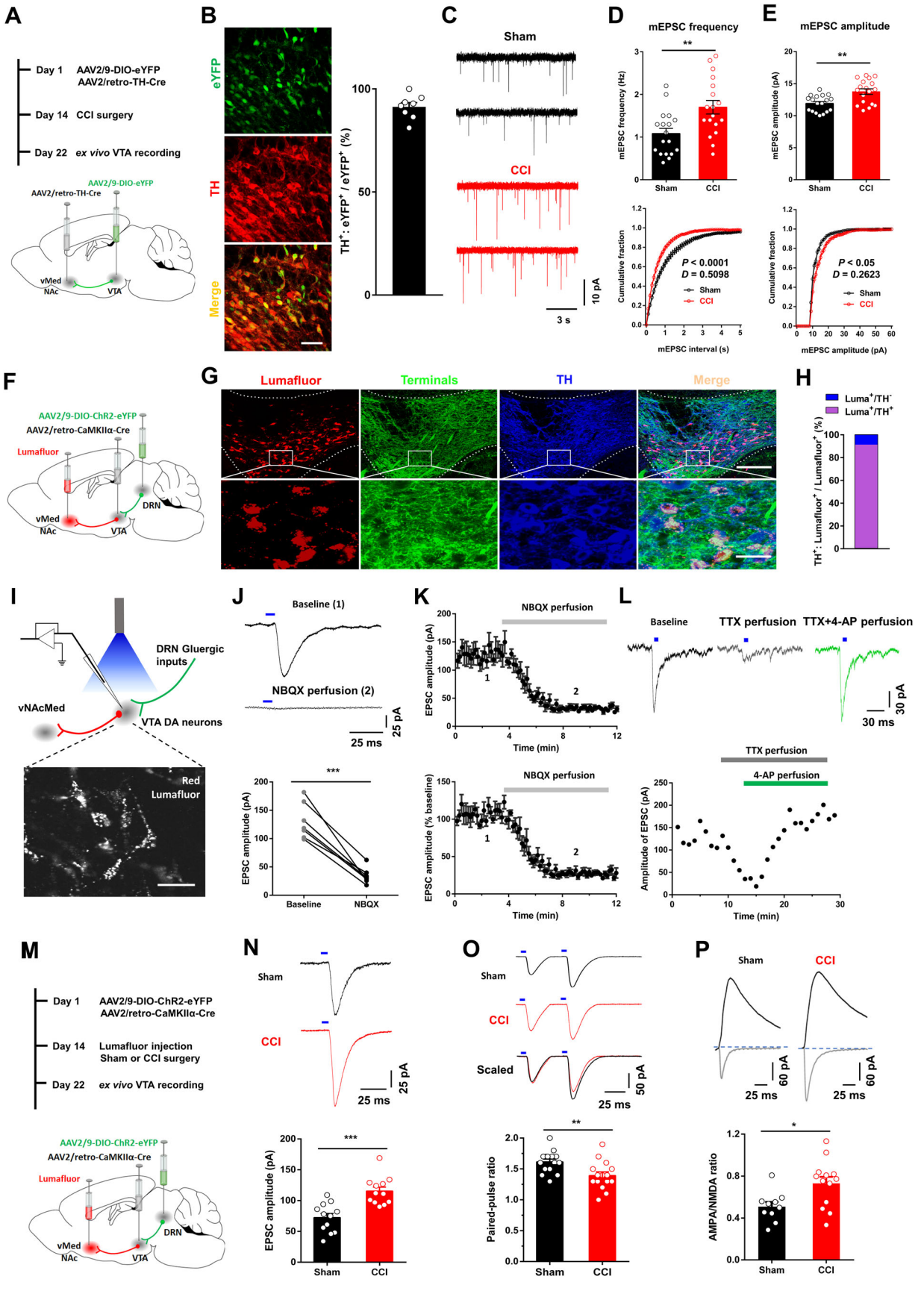

Figure 10. Continued.

mouse lines. Together, we extended these findings by establishing that the DRN glutamatergic, but not serotonergic, neurons constitute a pain-presentation input to the VTA dopamine system.

Although DRN serotonergic neurons are reported to innervate the VTA (Liu et al., 2014), studies also show that the VTA preferably receives dense innervation from DRN glutamatergic neurons (Hioki et al., 2010; McDevitt et al., 2014; Qi et al., 2014). Importantly, DRN SERT-expressing neurons established both asymmetric and symmetric synapses on VTA neurons, suggesting that some DRN SERT neurons coreleased glutamate and serotonin (Wang et al., 2019). It was previously shown that, within the total population of DRN glutamatergic and serotonergic neurons innervating the VTA, most were VGluT3-positive neurons (~82%) with minor populations of serotonin neurons (~37%) or dual VGluT3-serotonin neurons (~19%) (Qi et al., 2014). However, VGluT3-serotonin neurons established synapses on both VTA dopamine and nondopamine neurons (Wang et al., 2019). Duo to the neural heterogeneity and the local synapses between dopamine and nondopamine neurons in the VTA (Chaudhury et al., 2013; Morales and Margolis, 2017), the extent to which the VTA correspond to DRN glutamate- and serotonin-expressing neurons to encode pain modulation is still unclear. Our data showed that bilateral manipulation of DRN serotonin neurons projecting to the VTA could not change pain-like behaviors in mice, which partially indicated the exclusive involvement of DR glutamatergic neurons in pain modulation. Further research might gain a comprehensive understanding of how the VTA dopamine neurons integrated DRN glutamate-serotonin inputs during pain hypersensitivity.

Previous studies show that stimulation of DRN-VTA neurons with optogenetics is rewarding (McDevitt et al., 2014; Qi et al., 2014). There seemed to be a paradox because we found that activating this pathway derived pain behaviors. Research methodology might potentially contribute to this discrepancy. We found that mechanical stimulation of the hindpaw with 0.4 g, not 0.16 g, filament increased the withdrawal frequencies only in sham-operated mice with activation of the DRN-VTA pathway. Furthermore, in agreement with the rewarding nature of activating the DRN-VTA pathway, conditioning with nonpainful mechanical stimulation (0.16 g fiber) and CNO injection induced CPP in mice with hM3Dq expressed in DRN-VTA neurons. Interestingly, conditioning with mechanical stimulation (0.4 g fiber) and chemogenetic activation of the DRN-VTA pathway decreased the CPP score. These data indicate that the evoked pain responses during activating of the DRN-VTA pathway are aversive, despite that this circuit drive reward behaviors in normal conditions. Conversely, chemogenetic inhibition of DRN-VTA glutamatergic neurons attenuates pain hypersensitivity and induces CPP in CCI mice, supportive of the observation that relief of pain is rewarding and elicits negative reinforcement (King et al., 2009; Donnelly et al., 2021). These findings indicate that the firing activity of DRN-VTA glutamatergic neurons and the subsequent encoding of reward or aversion are highly context-dependent. The discrepancy might be additionally produced by differences in optogenetic tools, labeling efficiency, and stimulation parameters. For example, we used brief stimulation of DRN neurons, whereas other studies used slightly stronger stimulation parameters (McDevitt et al., 2014; Wang et al., 2019). Analyzing the roles of the various neural circuits within the reward system might provide further insights into the cellular and circuit mechanisms of reward versus pain processing.

The regulatory roles of DRN glutamatergic neurons in pain sensation show clear projection-pathway specificity. Although optogenetic manipulation of DRN-VTA^{DA}-vNAcMed pathways induced bidirectional modulation of pain responses, the DRN neurons targeting the vNAcMed did not contribute significantly to pain sensation. We, therefore, proposed that DRN neurons might process pain signals by innervating the VTA DA neurons, whose direct activation is responsible for pain hypersensitivity (Marinelli et al., 2005; Navratilova et al., 2012; Zhang et al., 2017; Liu et al., 2018). Given the differential roles of heterogeneous NAc neurons in pain processing (Ren et al., 2016), the indirect DRN-VTA^{DA}-vNAcMed pathway and the direct DRN-vNAcMed pathway might innervate distinct subpopulations of NAc neurons to mediate different roles in pain regulation. Future studies are needed to unmask how pain signals are encoded in the complex circuitry of the NAc.

VTA dopaminergic neurons receive glutamatergic inputs from several brain areas (Charara et al., 1996; Lammel et al., 2012; Kempadoo et al., 2013; Beier et al., 2015; Yang et al., 2018). Due to differences in synaptic connectivity, glutamatergic inputs to VTA from the lateral habenula and the laterodorsal tegmentum mediate diverse behavioral abnormalities (Lammel et al., 2012), indicating that clarifying the contribution of

←

Figure 10. Neuropathic pain induces potentiation of glutamatergic synaptic transmission onto VTA^{DA}-vNAcMed neurons. ***A***, Experimental timeline and schematic for investigating the mEPSC in VTA^{DA}-vNAcMed neurons from sham versus CCI mice. ***B***, Confocal image and quantification showed co-expression of eYFP in TH-positive DA cells ($n = 2$ sections from $n = 4$ mice). Scale, 25 µm. ***C***, mEPSC traces from VTA^{DA}-vNAcMed neurons in acute VTA slices of sham (black) and CCI (red) group mice. ***D***, Average values (top panel) and cumulative distributions (bottom panel) of mEPSC frequency in VTA^{DA}-vNAcMed neurons from sham and CCI mice (two-tailed t test, $t_{34} = 3.09$, $^{**}p = 0.004$; Two-sample Kolmogorov–Smirnov test, $^{***}p < 0.001$; $n = 18$ for each group). ***E***, Average values (top panel) and cumulative distributions (bottom panel) of mEPSC amplitude of VTA^{DA}-vNAcMed neurons from sham and CCI mice (two-tailed t test, $t_{34} = 3.487$, $^{**}p = 0.0014$; Two-sample Kolmogorov–Smirnov test, $^{*}p = 0.0301$; $n = 18$ for each group). ***F***, Schematic showing intracranial injection of viruses and retrobeads. ***G***, Representative images (top panel) showed that the majority of retrobeads-labeled VTA neurons were TH$^+$, and these neurons were surrounded by the eYFP-positive dense terminals from the DRN. Scale, 100 µm. Enlarged box (bottom panel) showing single and double staining. Scale, 25 µm. ***H***, Quantification showed 91.1% of retrobeads-expressing neurons were TH$^+$ ($n = 2$ sections from $n = 5$ mice). ***I***, Schematic diagram (top panel) showing the method of optogenetic stimulation and recording from Lumafluor$^+$ VTA^{DA}-vNAcMed neurons ex vivo. The representative image (bottom panel) showing Lumafluor$^+$ VTA neurons in a brain slice during patch-clamp recording. Scale, 25 µm. ***J***, Representative traces of EPSC in Lumafluor$^+$ VTA neurons evoked by optical stimulation of DRN terminals. Bath application of NBQX (5 µM) drastically decreased the optical EPSC amplitude (bottom panel) (paired t test, $t_6 = 8.639$, $^{***}p < 0.001$, $n = 7$ neurons). ***K***, Amplitude (top panel) and normalized amplitude (bottom panel) of optical EPSC of Lumafluor$^+$ VTA neurons obtained prior to and during NBQX (5 µM) application (gray). ***L***, Representative traces (top panel) and summarized time course (bottom panel) showed that the optical EPSC was eliminated by bath application of TTX (0.5 µM), and restored by 4-AP (100 µM). ***M***, Experimental timeline and schematic showing virus injection, surgeries, and electrophysiological recording. ***N***, Representative light-evoked EPSC traces (top panel) of VTA^{DA}-vNAcMed neurons from the sham group and CCI groups of mice. The amplitude of light-evoked EPSC was increased in CCI mice when compared with sham controls (two-tailed t test, $t_{22} = 4.589$, $^{***}p < 0.001$; $n = 12$ for each group). ***O***, Representative EPSC pairs (top panel) and group data (bottom panel) of VTA^{DA}-vNAcMed neurons evoked by two optogenetic stimuli (50 ms apart) in sham and CCI mice (two-tailed t test, $t_{28} = 2.952$, $^{**}p = 0.0063$; $n = 15$ neurons for each group). ***P***, Examples of AMPAR- and NMDAR-mediated light-evoked EPSCs in VTA^{DA}-vNAcMed neurons form CCI mice and sham controls. Summary showing increased AMPA/NMDA ratios at DRN-VTA synapses (two-tailed t test, $t_{21} = 2.709$, $^{*}p = 0.0132$; $n = 10$, 13 neurons). Data are represented as mean ± SEM.

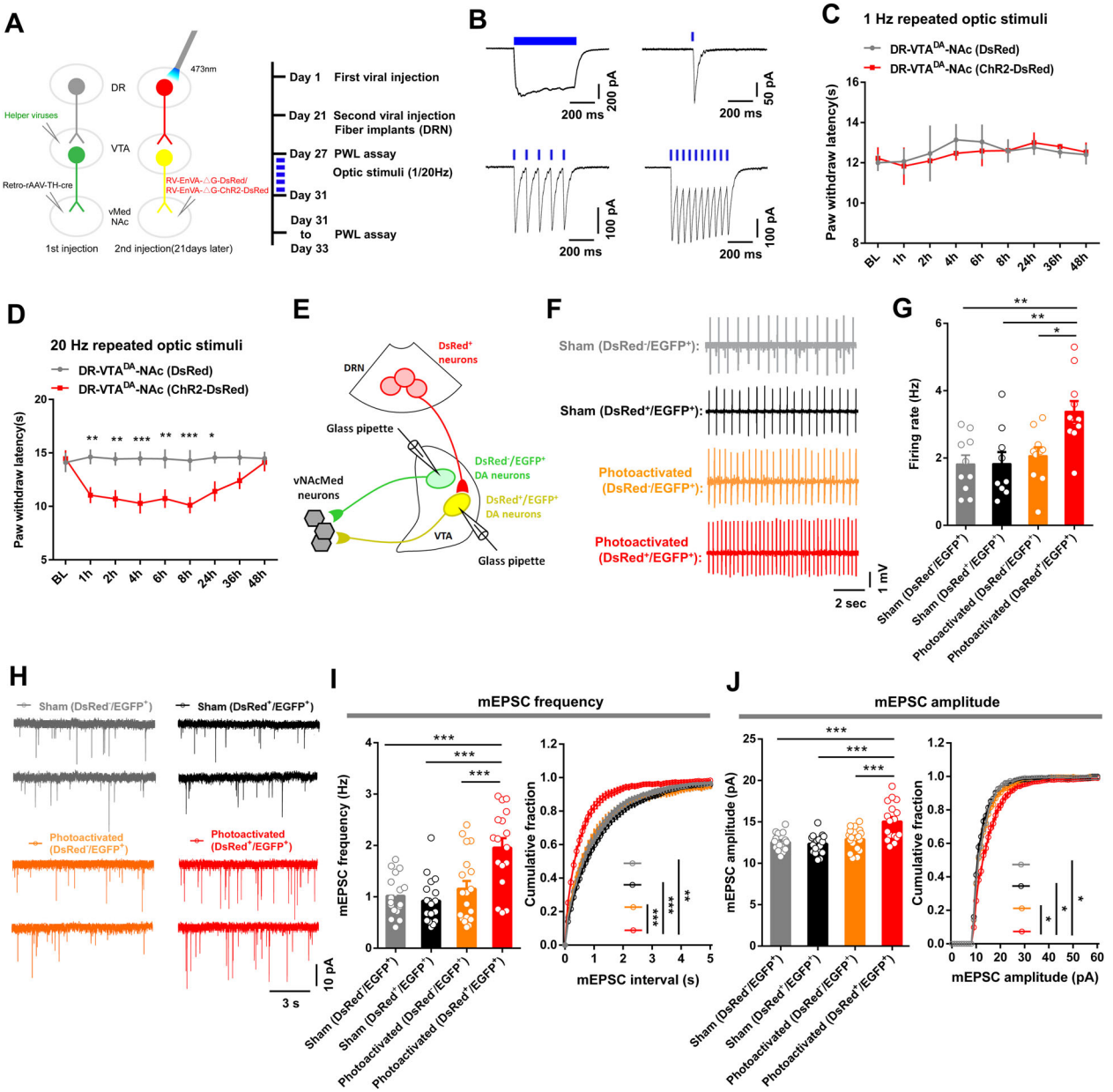

Figure 11. Repeated optical activation of DRN-VTA^{DA}-vNAcMed neurons and its effect on excitatory synaptic plasticity in VTA^{DA}-vNAcMed neurons. ***A***, Experimental schematic and timeline showing virus injection, optogenetic stimulation, and behavioral tests. ***B***, Whole-cell recording from ChR2-DsRed infected DRN neurons showed that long duration (500 ms) and short bursts (2, 10, or 20 Hz, 5 ms) of blue light illumination (473 nm) induced temporally precise photocurrents. ***C***, Repeated optical stimulation (1 Hz) of DRN-VTA^{DA}-vNAcMed neurons expressing ChR2-DsRed could not change the pain threshold in sham mice when compared with those expressed DsRed controls (two-way repeated measures ANOVA, group × epoch interaction, $F_{8,48} = 0.1968$, $p = 0.990$, $n = 4$ mice/group). ***D***, Repeated optical stimulation (20 Hz) of DRN-VTA^{DA}-vNAcMed neurons reduced the pain threshold in sham-operated mice, an effect lasting for 24 h at least (two-way repeated measures ANOVA, group × epoch interaction, $F_{8,128} = 3.624$, $p < 0.001$; Bonferroni's multiple-comparisons test, $^*p < 0.05$, $^{**}p < 0.01$, $^{***}p < 0.001$, $n = 9$ mice/group). ***E***, Schematic illustrating whole-cell recording of VTA^{DA}-vNAcMed neurons innervated by DRN neurons (DsRed$^+$/EGFP$^+$) or not (DsRed$^-$/EGFP$^+$). ***F,G***, Sample traces (***F***) and comparison (***G***) of spontaneous firing in DsRed$^-$/EGFP$^+$ and DsRed$^+$/EGFP$^+$ VTA^{DA}-vNAcMed neurons from mice received repeated optogenetic stimulation and their controls (one-way ANOVA, $F_{3,36} = 6.689$, $p = 0.0011$; *post hoc* Tukey's analysis, $^*p < 0.05$, $^{**}p < 0.01$, $n = 9$–11 neurons). ***H***, mEPSC traces from VTA^{DA}-vNAcMed neurons in acute VTA slices of sham mice and those subjected to repeated optogenetic stimulation. ***I***, Group data (left panel) and distribution plots (right panel) of mEPSC frequency of DsRed$^-$/EGFP$^+$ and DsRed$^+$/EGFP$^+$ VTA DA neurons from mice without or with repeated optogenetic stimulation of DRN-VTA^{DA}-vNAcMed neurons (for group data, one-way ANOVA, $F_{3,68} = 11.43$, $p < 0.001$, *post hoc* Tukey's analysis, $^{***}p < 0.001$; for distribution plots, Kruskal–Wallis test, $p < 0.001$; Dunn's multiple-comparisons test, $^{**}p < 0.01$, $^{***}p < 0.001$, $n = 17$–19 neurons). ***J***, Group data (left panel) and cumulative probability (right panel) of mEPSC amplitude from VTA^{DA}-vNAcMed neurons of each group (for group data, one-way ANOVA, $F_{3,68} = 12.32$, $p < 0.001$, *post hoc* Tukey's analysis, $^{***}p < 0.001$; for cumulative probability, Kruskal–Wallis test, $p < 0.01$; Dunn's multiple-comparisons test, $^*p < 0.05$, $n = 17$–19 neurons). Data are represented as mean ± SEM.

selective inputs to VTA is important for a better understanding of their role in pain processing. In this regard, we found enhanced presynaptic glutamate release and VTA glutamatergic receptor functions in CCI mice. Furthermore, this synaptic plasticity might underly the algesic effect of DRN-VTA^{DA}-vNAcMed neurons, as repeated optogenetic stimulation of these neurons on the one hand enhanced excitatory synaptic functions, on the other hand, induced firing abnormalities as reported in previous studies in VTA^{DA}-NAc neurons (Marinelli et al., 2005; Zhang et al., 2017; Liu et al., 2018). Notably, as evidenced by

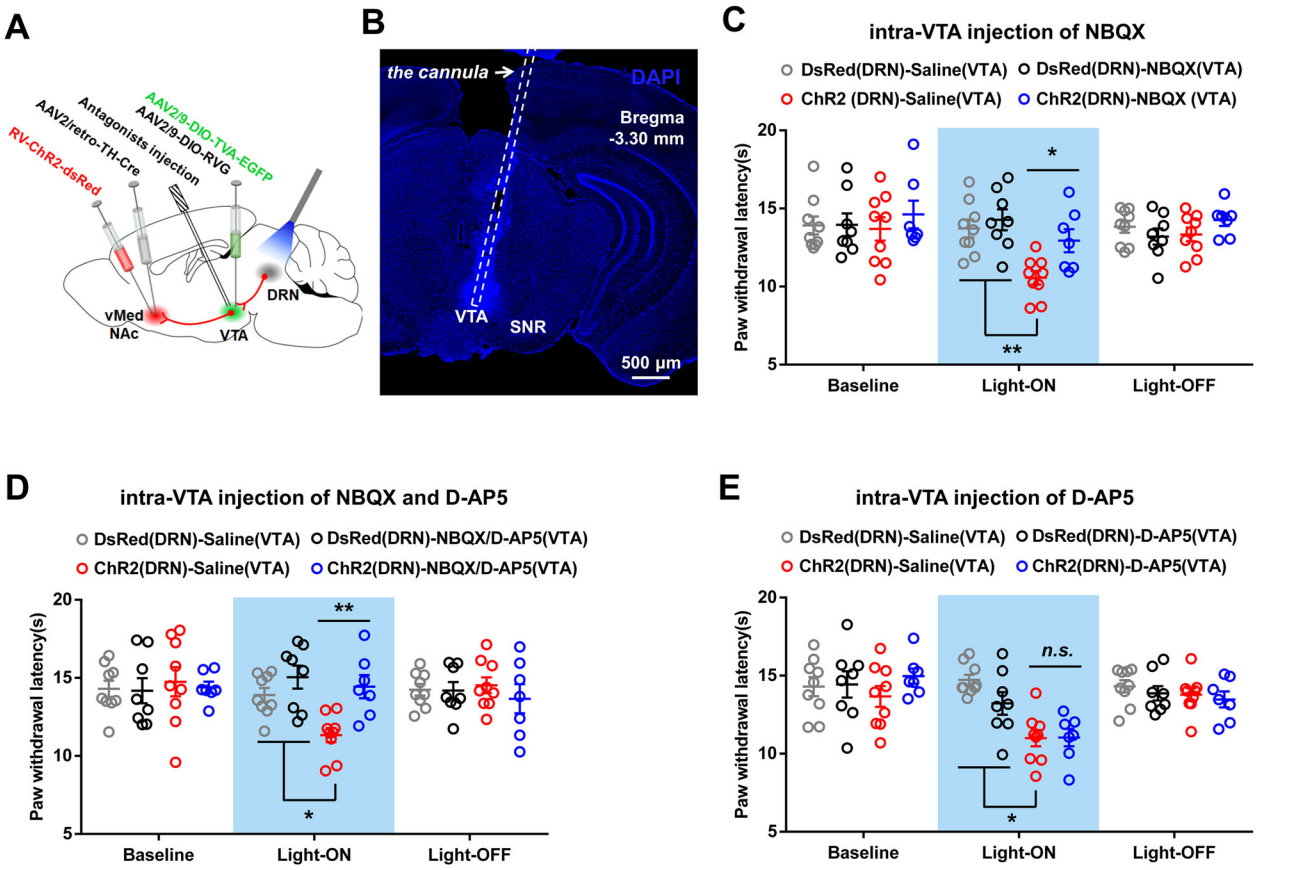

Figure 12. Effect of blocking glutamate receptors in VTA on the algesic effect produced by optical stimulation of DRN-VTA^{DA}-vNAcMed neurons. ***A***, Experimental timeline and schematic showing surgeries, antagonist infusion, and optical stimulation. ***B***, A representative image revealing the cannula implantation into the VTA for antagonist infusion. Scale, 500 μm. ***C–E***, The reduced thermal paw withdrawal latencies in sham mice induced by optical stimulation of DRN-VTA^{DA}-vNAcMed pathways were blocked by intra-VTA pretreatment with AMPA-receptor antagonist alone (***C***) or a combination of AMPA- and NMDA-receptor antagonist (***D***), but not NMDA-receptor antagonist (***E***) (two-way repeated measure ANOVA, group × time interaction, $F_{6,58} = 6.095$, $p < 0.001$ for NBQX injection; group × time interaction, $F_{6,58} = 4.046$, $p = 0.0019$ for NBQX and D-AP5 infusion; group × time interaction, $F_{6,58} = 5.081$, $p < 0.001$ for D-AP5 administration; *post hoc* Bonferroni's analysis, $^{*}p < 0.05$, $^{**}p < 0.01$, $n = 7–9$ mice/group). SNR, reticular part of the substantia nigra. Data are represented as mean ± SEM.

alterations in neuronal activity in lesion experiments, there were reciprocal relationships between the DRN serotonin and VTA DA neurons (Hamon and Blier, 2013). Selective lesion of DA neurons decreased the spontaneous firing activity of DRN serotonin neurons by 60% in vivo (Guiard et al., 2008). Conversely, the selective lesion of serotonin neurons enhanced by 36% the firing activity of VTA DA neurons (Guiard et al., 2008). Partially consistent with these findings, it was reported that optical stimulation of serotonergic fibers induced neuronal excitation and neuronal inhibition of VTA neurons (Wang et al., 2019). The DRN serotonin neurons innervated dopamine and nondopamine neuron in the VTA. Furthermore, the VTA GABA and glutamate neurons also established local synapses onto VTA dopamine neurons (Morales and Margolis, 2017), whose activity might be differentially regulated by serotonin inputs.

The enhanced activities of VTA dopamine neurons are demonstrated in rodents with neuropathic pain and human volunteers received painful stimulation (Lee et al., 2008; Brischoux et al., 2009; Sagheddu et al., 2015; Zhang et al., 2017). By contrast, patch-clamp recordings reveal lower firing rates in VTA neurons in mice with chronic pain (Ren et al., 2016; Watanabe et al., 2018). One possible explanation for these discrepancies is the significant heterogeneity in the anatomy and function of midbrain dopamine neurons (Brischoux et al., 2009; Chaudhury et al., 2013; Tye et al., 2013). For example, the activity of DA neurons in the lateral VTA is decreased after nerve injury. However, a higher degree of excitability of medial VTA DA neurons is found in mice with neuropathic pain (Huang et al., 2019b). Importantly, dopamine neurons that project to the NAcMed are mainly located in the medial posterior VTA (Lammel et al., 2011). For the NAcMed, DA terminals in the vNAcMed were excited, yet DA terminals in the dNAcMed were inhibited, in mice that received painful stimuli (de Jong et al., 2019). In support of these findings, our data indicated that the VTA^{DA}-vNAcMed neurons were activated, while the VTA^{DA}-dNAcMed neurons showed a tendency to be suppressed, in response to neuropathic pain. Importantly, dopamine neurons located in the ventral VTA are excited by noxious stimuli, in contrast to dorsal VTA dopamine neurons, which are inhibited (Brischoux et al., 2009). This provides additional support for the importance of the projection specificity of mesolimbic circuits in pain processing. Additionally, the discrepancy in results could be obtained with different animal models.

Collectively, we provide a highly consistent and comprehensive cellular, neural circuit, and behavioral evidence for the underlying mechanisms by which the DRN-VTA^{DA}-vNAcMed pathway facilitates pain sensation. Our data uncover a previously unknown role of the DRN neural pathway in pain regulation.

References

Andersen E, Dafny N (1983) Dorsal raphe stimulation reduces responses of parafascicular neurons to noxious stimulation. Pain 15:323–331.

Baker KG, Halliday GM, Tork I (1990) Cytoarchitecture of the human dorsal raphe nucleus. J Comp Neurol 301:147–161.

Baliki MN, Apkarian AV (2015) Nociception, pain, negative moods, and behavior selection. Neuron 87:474–491.

Baliki MN, Geha PY, Fields HL, Apkarian AV (2010) Predicting value of pain and analgesia: nucleus accumbens response to noxious stimuli changes in the presence of chronic pain. Neuron 66:149–160.

Becerra L, Breiter HC, Wise R, Gonzalez RG, Borsook D (2001) Reward circuitry activation by noxious thermal stimuli. Neuron 32:927–946.

Beier KT, Steinberg EE, DeLoach KE, Xie S, Miyamichi K, Schwarz L, Gao XJ, Kremer EJ, Malenka RC, Luo L (2015) Circuit architecture of VTA dopamine neurons revealed by systematic input-output mapping. Cell 162: 622–634.

Borges GS, Berrocoso E, Ortega-Alvaro A, Mico JA, Neto FL (2013) Extracellular signal-regulated kinase activation in the chronic constriction injury model of neuropathic pain in anaesthetized rats. Eur J Pain 17:35–45.

Brischoux F, Chakraborty S, Brierley DI, Ungless MA (2009) Phasic excitation of dopamine neurons in ventral VTA by noxious stimuli. Proc Natl Acad Sci U S A 106:4894–4899.

Callaway EM, Luo L (2015) Monosynaptic circuit tracing with glycoprotein-deleted rabies viruses. J Neurosci 35:8979–8985.

Charara A, Smith Y, Parent A (1996) Glutamatergic inputs from the pedunculopontine nucleus to midbrain dopaminergic neurons in primates: phaseolus vulgaris-leucoagglutinin anterograde labeling combined with postembedding glutamate and GABA immunohistochemistry. J Comp Neurol 364:254–266.

Chaudhury D, et al. (2013) Rapid regulation of depression-related behaviours by control of midbrain dopamine neurons. Nature 493:532–536.

Chen G, Park CK, Xie RG, Ji RR (2015) Intrathecal bone marrow stromal cells inhibit neuropathic pain via TGF-beta secretion. J Clin Invest 125: 3226–3240.

Cohen SP, Mao JR (2014) Neuropathic pain: mechanisms and their clinical implications. BMJ 348:f7656.

Cohen SP, Vase L, Hooten WM (2021) Chronic pain: an update on burden, best practices, and new advances. Lancet 397:2082–2097.

De Gregorio D, McLaughlin RJ, Posa L, Ochoa-Sanchez R, Enns J, Lopez-Canul M, Aboud M, Maione S, Comai S, Gobbi G (2019) Cannabidiol modulates serotonergic transmission and reverses both allodynia and anxiety-like behavior in a model of neuropathic pain. Pain 160:136–150.

de Jong JW, Afjei SA, Pollak Dorocic I, Peck JR, Liu C, Kim CK, Tian L, Deisseroth K, Lammel S (2019) A neural circuit mechanism for encoding aversive stimuli in the mesolimbic dopamine system. Neuron 101:133–151.

Deng J, et al. (2020) The parabrachial nucleus directly channels spinal nociceptive signals to the intralaminar thalamic nuclei, but not the amygdala. Neuron 107:909–923.

Deshpande A, Bergami M, Ghanem A, Conzelmann KK, Lepier A, Gotz M, Berninger B (2013) Retrograde monosynaptic tracing reveals the temporal evolution of inputs onto new neurons in the adult dentate gyrus and olfactory bulb. Proc Natl Acad Sci U S A 110:E1152–1161.

Di Castro MA, Trettel F, Milior G, Maggi L, Ragozzino D, Limatola C (2016) The chemokine CXCL16 modulates neurotransmitter release in hippocampal CA1 area. Sci Rep 6:34633.

Donnelly CR, et al. (2021) STING controls nociception via type I interferon signalling in sensory neurons. Nature 591:275–280.

Duggan AW, Griersmith BT (1979) Inhibition of the spinal transmission of nociceptive information by supraspinal stimulation in the cat. Pain 6: 149–161.

Felix-Ortiz AC, Beyeler A, Seo C, Leppla CA, Wildes CP, Tye KM (2013) BLA to vHPC inputs modulate anxiety-related behaviors. Neuron 79:658–664.

Gear RW, Levine JD (2011) Nucleus accumbens facilitates nociception. Exp Neurol 229:502–506.

Guiard BP, El Mansari M, Merali Z, Blier P (2008) Functional interactions between dopamine, serotonin and norepinephrine neurons: an in-vivo electrophysiological study in rats with monoaminergic lesions. Int J Neuropsychopharmacol 11:625–639.

Gunaydin LA, et al. (2014) Natural neural projection dynamics underlying social behavior. Cell 157:1535–1551.

Hamon M, Blier P (2013) Monoamine neurocircuitry in depression and strategies for new treatments. Prog Neuropsychopharmacol Biol Psychiatry 45:54–63.

Han Q, et al. (2016) SHANK3 deficiency impairs heat hyperalgesia and TRPV1 signaling in primary sensory neurons. Neuron 92:1279–1293.

Hargreaves K, Dubner R, Brown F, Flores C, Joris J (1988) A new and sensitive method for measuring thermal nociception in cutaneous hyperalgesia. Pain 32:77–88.

Hioki H, Nakamura H, Ma YF, Konno M, Hayakawa T, Nakamura KC, Fujiyama F, Kaneko T (2010) Vesicular glutamate transporter 3-expressing nonserotonergic projection neurons constitute a subregion in the rat midbrain raphe nuclei. J Comp Neurol 518:668–686.

Huang J, Gadotti VM, Chen L, Souza IA, Huang S, Wang D, Ramakrishnan C, Deisseroth K, Zhang Z, Zamponi GW (2019a) A neuronal circuit for activating descending modulation of neuropathic pain. Nat Neurosci 22:1659–1668.

Huang S, Borgland SL, Zamponi GW (2019b) Peripheral nerve injury-induced alterations in VTA neuron firing properties. Mol Brain 12:89.

Huang YH, et al. (2009) In vivo cocaine experience generates silent synapses. Neuron 63:40–47.

Imai S, Saeki M, Yanase M, Horiuchi H, Abe M, Narita M, Kuzumaki N, Suzuki T, Narita M (2011) Change in microRNAs associated with neuronal adaptive responses in the nucleus accumbens under neuropathic pain. J Neurosci 31:15294–15299.

Jacobs BL, Azmitia EC (1992) Structure and function of the brain serotonin system. Physiol Rev 72:165–229.

Kempadoo KA, et al. (2013) Hypothalamic neurotensin projections promote reward by enhancing glutamate transmission in the VTA. J Neurosci 33: 7618–7626.

King T, Vera-Portocarrero L, Gutierrez T, Vanderah TW, Dussor G, Lai J, Fields HL, Porreca F (2009) Unmasking the tonic-aversive state in neuropathic pain. Nat Neurosci 12:1364–1366.

Krishnan V, et al. (2007) Molecular adaptations underlying susceptibility and resistance to social defeat in brain reward regions. Cell 131:391–404.

Lammel S, Ion DI, Roeper J, Malenka RC (2011) Projection-specific modulation of dopamine neuron synapses by aversive and rewarding stimuli. Neuron 70:855–862.

Lammel S, Lim BK, Ran C, Huang KW, Betley MJ, Tye KM, Deisseroth K, Malenka RC (2012) Input-specific control of reward and aversion in the ventral tegmental area. Nature 491:212–217.

Lee MC, Zambreanu L, Menon DK, Tracey I (2008) Identifying brain activity specifically related to the maintenance and perceptual consequence of central sensitization in humans. J Neurosci 28:11642–11649.

Li C, Sugam JA, Lowery-Gionta EG, McElligott ZA, McCall NM, Lopez AJ, McKlveen JM, Pleil KE, Kash TL (2016) Mu opioid receptor modulation of dopamine neurons in the periaqueductal gray/dorsal raphe: a role in regulation of pain. Neuropsychopharmacology 41:2122–2132.

Lim G, Kim H, McCabe MF, Chou CW, Wang S, Chen LL, Marota JJ, Blood A, Breiter HC, Mao J (2014) A leptin-mediated central mechanism in analgesia-enhanced opioid reward in rats. J Neurosci 34: 9779–9788.

Liu D, et al. (2018) Brain-derived neurotrophic factor mediated projection-specific regulation of depressive-like and nociceptive behaviors in the mesolimbic reward circuitry. Pain 159:175–188.

Liu PF, et al. (2022) Modulation of itch and pain signals processing in ventrobasal thalamus by thalamic reticular nucleus. iScience 25:103625.

Liu Z, et al. (2014) Dorsal raphe neurons signal reward through 5-HT and glutamate. Neuron 81:1360–1374.

Lopez AJ, Kramar E, Matheos DP, White AO, Kwapis J, Vogel-Ciernia A, Sakata K, Espinoza M, Wood MA (2016) Promoter-specific effects of DREADD modulation on hippocampal synaptic plasticity and memory formation. J Neurosci 36:3588–3599.

Luo M, Zhou J, Liu Z (2015) Reward processing by the dorsal raphe nucleus: 5-HT and beyond. Learn Mem 22:452–460.

Marinelli S, Pascucci T, Bernardi G, Puglisi-Allegra S, Mercuri NB (2005) Activation of TRPV1 in the VTA excites dopaminergic neurons and increases chemical-and noxious-induced dopamine release in the nucleus accumbens. Neuropsychopharmacology 30:864–870.

Matthews GA, et al. (2016) Dorsal raphe dopamine neurons represent the experience of social isolation. Cell 164:617–631.

Mayer DJ, Price DD (1976) Central nervous system mechanisms of analgesia. Pain 2:379–404.

McDevitt RA, Tiran-Cappello A, Shen H, Balderas I, Britt JP, Marino RAM, Chung SL, Richie CT, Harvey BK, Bonci A (2014) Serotonergic versus nonserotonergic dorsal raphe projection neurons: differential participation in reward circuitry. Cell Rep 8:1857–1869.

Miyamichi K, Shlomai-Fuchs Y, Shu M, Weissbourd BC, Luo L, Mizrahi A (2013) Dissecting local circuits: parvalbumin interneurons underlie broad feedback control of olfactory bulb output. Neuron 80:1232–1245.

Morales M, Margolis EB (2017) Ventral tegmental area: cellular heterogeneity, connectivity and behaviour. Nat Rev Neurosci 18:73–85.

Navratilova E, Xie JY, Okun A, Qu CL, Eyde N, Ci S, Ossipov MH, King T, Fields HL, Porreca F (2012) Pain relief produces negative reinforcement through activation of mesolimbic reward–valuation circuitry. Proc Natl Acad Sci U S A 109:20709–20713.

Nissen NI, Anderson KR, Wang H, Lee HS, Garrison C, Eichelberger SA, Ackerman K, Im W, Miwa JM (2018) Augmenting the antinociceptive effects of nicotinic acetylcholine receptor activity through lynx1 modulation. PLoS One 13:e0199643.

Noack J, Murau R, Engelmann M (2015) Consequences of temporary inhibition of the medial amygdala on social recognition memory performance in mice. Front Neurosci 9:152.

Ossipov MH, Dussor GO, Porreca F (2010) Central modulation of pain. J Clin Invest 120:3779–3787.

Peirs C, Seal RP (2016) Neural circuits for pain: recent advances and current views. Science 354:578–584.

Petreanu L, Huber D, Sobczyk A, Svoboda K (2007) Channelrhodopsin-2-assisted circuit mapping of long-range callosal projections. Nat Neurosci 10:663–668.

Qi J, Zhang S, Wang HL, Wang H, de Jesus Aceves Buendia J, Hoffman AF, Lupica CR, Seal RP, Morales M (2014) A glutamatergic reward input from the dorsal raphe to ventral tegmental area dopamine neurons. Nat Commun 5:5390.

Qiao JT, Dafny N (1988) Dorsal raphe stimulation modulates nociceptive responses in thalamic parafascicular neurons via an ascending pathway: further studies on ascending pain modulation pathways. Pain 34:65–74.

Ren W, Centeno MV, Berger S, Wu Y, Na X, Liu X, Kondapalli J, Apkarian AV, Martina M, Surmeier DJ (2016) The indirect pathway of the nucleus accumbens shell amplifies neuropathic pain. Nat Neurosci 19:220–222.

Reyes-Vazquez C, Qiao JT, Dafny N (1989) Nociceptive responses in nucleus parafascicularis thalami are modulated by dorsal raphe stimulation and microiontophoretic application of morphine and serotonin. Brain Res Bull 23:405–411.

Reynolds DV (1969) Surgery in the rat during electrical analgesia induced by focal brain stimulation. Science 164:444–445.

Sagheddu C, et al. (2015) Enhanced serotonin and mesolimbic dopamine transmissions in a rat model of neuropathic pain. Neuropharmacology 97:383–393.

Segal M (1979) Serotonergic innervation of the locus coeruleus from the dorsal raphe and its action on responses to noxious stimuli. J Physiol 286:401–415.

Singh AK, Zajdel J, Mirrasekhian E, Almoosawi N, Frisch I, Klawonn AM, Jaarola M, Fritz M, Engblom D (2017) Prostaglandin-mediated inhibition of serotonin signaling controls the affective component of inflammatory pain. J Clin Invest 127:1370–1374.

Singhmar P, et al. (2016) Critical role for Epac1 in inflammatory pain controlled by GRK2-mediated phosphorylation of Epac1. Proc Natl Acad Sci U S A 113:3036–3041.

Stogsdill JA, Ramirez J, Liu D, Kim YH, Baldwin KT, Enustun E, Ejikeme T, Ji RR, Eroglu C (2017) Astrocytic neuroligins control astrocyte morphogenesis and synaptogenesis. Nature 551:192–197.

Tache Y, Amorim D, David-Pereira A, Marques P, Puga S, Rebelo P, Costa P, Pertovaara A, Almeida A, Pinto-Ribeiro F (2014) A role of supraspinal galanin in behavioural hyperalgesia in the rat. PLoS One 9:e113077.

Taves S, Berta T, Liu DL, Gan S, Chen G, Kim YH, Van de Ven T, Laufer S, Ji RR (2016) Spinal inhibition of p38 MAP kinase reduces inflammatory and neuropathic pain in male but not female mice: sex-dependent microglial signaling in the spinal cord. Brain Behav Immun 55:70–81.

Tye KM, et al. (2013) Dopamine neurons modulate neural encoding and expression of depression-related behaviour. Nature 493:537–541.

Vasudeva RK, Lin RC, Simpson KL, Waterhouse BD (2011) Functional organization of the dorsal raphe efferent system with special consideration of nitrergic cell groups. J Chem Neuroanat 41:281–293.

Vong L, Ye C, Yang Z, Choi B, Chua S Jr, Lowell BB (2011) Leptin action on GABAergic neurons prevents obesity and reduces inhibitory tone to POMC neurons. Neuron 71:142–154.

Wager TD, Scott DJ, Zubieta JK (2007) Placebo effects on human mu-opioid activity during pain. Proc Natl Acad Sci U S A 104:11056–11061.

Wall NR, Wickersham IR, Cetin A, De La Parra M, Callaway EM (2010) Monosynaptic circuit tracing in vivo through Cre-dependent targeting and complementation of modified rabies virus. Proc Natl Acad Sci U S A 107:21848–21853.

Walsh JJ, Christoffel DJ, Heifets BD, Ben-Dor GA, Selimbeyoglu A, Hung LW, Deisseroth K, Malenka RC (2018) 5-HT release in nucleus accumbens rescues social deficits in mouse autism model. Nature 560:589–594.

Wang HL, et al. (2019) Dorsal raphe dual serotonin-glutamate neurons drive reward by establishing excitatory synapses on VTA mesoaccumbens dopamine neurons. Cell Rep 26:1128–1142.

Watabe-Uchida M, Zhu L, Ogawa SK, Vamanrao A, Uchida N (2012) Whole-brain mapping of direct inputs to midbrain dopamine neurons. Neuron 74:858–873.

Watanabe M, et al. (2018) Activation of ventral tegmental area dopaminergic neurons reverses pathological allodynia resulting from nerve injury or bone cancer. Mol Pain 14:1–11.

Woo CW, Roy M, Buhle JT, Wager TD (2015) Distinct brain systems mediate the effects of nociceptive input and self-regulation on pain. PLoS Biol 13: e1002036.

Wood PB (2006) Mesolimbic dopaminergic mechanisms and pain control. Pain 120:230–234.

Xu S, Das G, Hueske E, Tonegawa S (2017) Dorsal raphe serotonergic neurons control intertemporal choice under trade-off. Curr Biol 27: 3111–3119.

Xu ZZ, Zhang L, Liu T, Park JY, Berta T, Yang R, Serhan CN, Ji RR (2010) Resolvins RvE1 and RvD1 attenuate inflammatory pain via central and peripheral actions. Nat Med 16:592–597.

Xu ZZ, Kim YH, Bang S, Zhang Y, Berta T, Wang F, Oh SB, Ji RR (2015) Inhibition of mechanical allodynia in neuropathic pain by TLR5-mediated a-fiber blockade. Nat Med 21:1326–1331.

Yang Y, Cui Y, Sang K, Dong Y, Ni Z, Ma S, Hu H (2018) Ketamine blocks bursting in the lateral habenula to rapidly relieve depression. Nature 554:317–322.

Yu W, Pati D, Pina MM, Schmidt KT, Boyt KM, Hunker AC, Zweifel LS, McElligott ZA, Kash TL (2021) Periaqueductal gray/dorsal raphe dopamine neurons contribute to sex differences in pain-related behaviors. Neuron 109:1365–1380.

Zhang H, et al. (2017) Brain-derived neurotrophic factor in the mesolimbic reward circuitry mediates nociception in chronic neuropathic pain. Biol Psychiatry 82:608–618.

Zhang Z, Pan ZZ (2010) Synaptic mechanism for functional synergism between delta- and mu-opioid receptors. J Neurosci 30:4735–4745.

Zhou W, Cheung K, Kyu S, Wang L, Guan Z, Kurien PA, Bickler PE, Jan LY (2018) Activation of orexin system facilitates anesthesia emergence and pain control. Proc Natl Acad Sci U S A 115:10740–10747.

Zhou Z, et al. (2019) A VTA GABAergic neural circuit mediates visually evoked innate defensive responses. Neuron 103:473–488.